

# Distinguishing Black Hole and Naked Singularity in MOG via Inertial Frame Dragging Effect

Parthapratim Pradhan\*

*Department of Physics*

*Hiralal Mazumdar Memorial College For Women*

Dakshineswar, Kolkata-700035, India

## Abstract

We analyze the generalized spin precession of a test gyroscope around a stationary spacetime i.e. for Kerr-MOG black hole (BH) in scalar-tensor-vector gravity or modified gravity (MOG). A detailed study of generalized spin frequency has been done for *non* extremal Kerr-MOG BH, *extremal* Kerr-MOG BH and *naked singularity* (NS) in comparison to non-extremal BH, extremal BH and NS of Kerr spacetime. The generalized spin frequency that we have computed could be expressed in terms of the BH mass parameter, the angular momentum parameter and the MOG parameter. Moreover, we differentiate the non extremal BH, extremal BH and NS via computation of the said precession frequency. The Lense-Thirring (LT) frequency can obtain from generalized spin frequency by taking the limit as  $\Omega = 0$  i. e. when the angular frequency is set to zero limit. Furthermore, we compute the LT frequency for various values of angular coordinates i.e. starting from polar to the equatorial plane. We show that the LT frequency diverges at the horizon for extremal BH. Finally, we study the accretion disk physics by computing three epicyclic frequencies namely the Keplerian frequency, the radial epicyclic frequency and the vertical epicyclic frequency. We also compute the periastron frequency and nodal frequency. With the aid of these frequency profiles, one can distinguish three compact objects i. e. *non-extremal BH*, *extremal BH* and *NS*.

## 1 Introduction:

The de-Sitter precession [1] and the Lense-Thirring (LT) precession [2] are two extraordinary effects predicted by Einstein's general theory of relativity <sup>1</sup>. They are directly measured by Gravity Probe-B experiment: a space experiment to test the general theory of relativity (GTR) [5]. It was initiated and launched by NASA in 2004. The satellite consists of four gyroscopes and a telescope orbiting 642 km or around 400 mile above the Earth [4]. Another important satellite i. e. Rossi X-ray Timing Explorer (RXTE) [6] was launched by NASA in 1995 which help us to confirm the existence of the frame-dragging effect which was predicted by Einstein's gravity. It was also detected the X-rays from different compact objects like BHs, neutron stars and X-ray pulsars etc. The effects of frame dragging effect on the galactic-center stars and kinematic properties was investigated in [8]. The measurement of the gyroscopic precession and its implications was discussed in [9].

There are several important tests [10, 11, 12] of GTR which was carried out by different space mission experiment. For example, (a) the weak equivalence principle: the basis of geometrical theories of gravity which was tested by Lunar laser ranging of accuracy in the order of  $10^{-13}$ . (b) The strong equivalence principle: the cornerstone of the GTR which was tested by the lunar laser ranging of accuracy  $< 10^3$ . The gravitational time dilation or gravitational red-shift which was experimentally verified by Gravity Probe-A. The Shapiro time-delay which was also experimentally tested by very long baseline interferometry (VLBI) [10].

---

\*pppradhan77@gmail.com

<sup>1</sup>The possible new experimental test of Einstein's general theory of relativity was first proposed by Schiff in 1960 [3].

Moreover, the perihelion advance of mercury which was tested by the mercury radar ranging method and the accuracy of the order of  $10^{-3}$ . The periastron advance, time dilation, time delay and the rate of change of orbital period which was verified by binary pulsar PSR 1913+16. The geodetic precession or de-Sitter effect which was tested by the lunar laser ranging of accuracy in the order of  $6 \times 10^{-3}$  and using Gravity Probe-B. Finally, the LT effect or the frame-dragging effect was experimentally confirmed by using laser geodynamics satellite (LAGEOS) [13]<sup>2</sup> and LAGEOS2<sup>3</sup> of accuracy in the order of  $10^{-1}$ .

The de-Sitter precession or geodetic effect is the dragging of a gyroscope due to its motion in a static gravitational field. Whereas the LT precession or frame-dragging effect of a gyroscope is due to the rotation of a massive body. In the weak field limit, such LT precession frequency is defined as [14]

$$\vec{\Omega}_{LT} = \frac{G}{c^2 r^3} \left[ 3 \left( \vec{J} \cdot \hat{r} \right) \hat{r} - \vec{J} \right] \quad (1)$$

where,  $\hat{r}$  is the unit vector along angular momentum  $\vec{J}$  direction,  $G$  is Newton's gravitational constant and  $c$  is the speed of light. Earlier derivations of the LT frequency [14] in the literature was considered on the weak field approximation by assuming  $r > M$  ( $M$  is Arnowitt-Deser-Misner (ADM) mass of any compact object) i. e. large distances for the test gyroscope. Now the question should be arise naturally what would be the LT precession frequency in the strong gravity regime? This is one of the prime motivation behind this work.

In the strong gravity limit, the LT frequency for Kerr BH and Kerr-Taub-NUT (Newman-Unti-Tamburino) BH was explicitly derived in [17]. In this work, the authors showed the role of NUT parameter in inertial frame dragging effect. It was shown there that the LT frequency does not vanish for Taub-NUT spacetime when the value of angular momentum vanishes. Similarly for axisymmetric NUT spacetime, the result becomes more prominent when the value of ADM mass parameter does vanish. The LT frequency for more generalized class of spacetimes like Plebański and Demiański in the strong field limit was explicitly discussed in [18]. The authors in [19] studied the inertial frame dragging effect of a rotating traversable wormhole. In his work, he also described the behavior of a test gyroscope when it moves towards a spinning traversable wormhole. Moreover, they derived the LT frequency for this wormhole and showed that the LT frequency diverges on the ergosphere. Along the pole, the LT frequency is inversely proportional to the spin parameter of the wormhole.

In [20], the authors derived the LT frequency inside a rotating neutron star. Where the authors showed that the LT frequency rate along the pole decreases from the center to the surface of the neutron star. Along the equatorial plane the LT frequency rate decreases initially away from the center and approaches a small value in the surface. Morsink and Stella [22] first showed that the precession frequency of a rotating neutron star could be expressed in terms of orbital frequency which was observed at infinity. They also computed the precession frequencies of circular orbits around rapidly spinning neutron stars for a variety of masses and the equation of state. One should consult a good review on inertial frame-dragging effect which would be found in Ref. [12]. Also one could found the history of the Lense-Thirring effect in Ref. [15]. Gyroscope precession along equatorial plane of stable orbits for Kerr BH could be found in [16].

However, the LT precession frequency of various axisymmetric BHs including the analogue space-time and neutron star [17, 18, 19, 20, 24] are computed so far but till date the LT frequency and the generalized spin frequency are not considered for Kerr-MOG(KMOG) BH. In the present manuscript, we wish to derive the generalized spin frequency of KMOG BH. It is a kind of BH solution in the scalar-tensor-vector gravity (STVG) or simply it is known as MOG. This theory was first proposed by Moffat [25, 27, 28, 29, 30, 31]. The fundamental features of this theory as follows. It correctly explains various kind of astronomical observations: dynamics of galaxies and cluster of galaxies, bullet clusters, galaxy rotation curves, the amount of luminous matter, the exotic dark matter and the acceleration of the universe etc.

---

<sup>2</sup>It was launched by NASA in 1976.

<sup>3</sup>This satellite was launched in 1992 by Italian space agency and NASA.

The MOG gravity is a type of alternative theory of gravity. It contains scalar field and massive vector field. The action in STVG theory consists of scalar action and vector action hence it modifies the Einstein-Hilbert action. The MOG theory is formulated via MOND phenomenology in the weak field approximation. Most importantly, this theory correctly explains the observations of the solar system [26]. It could also be used to describe the growth of the structure of the universe, the power spectrum of the matter and the acoustical power spectrum of the cosmic microwave background (CMB) data. It should be noted that various features of MOG like superradiance, quasinormal modes, thermodynamics, geodesics properties, orbital and vertical epicyclic frequencies, Penrose process, gravitational bending of light, BH shadow and BH merger estimates etc. are studied in [25, 26, 27, 28, 29, 30, 31, 32, 33, 34, 35] respectively.

The fundamental postulate in MOG theory is that the BH charge parameter is proportional to the Komar mass i. e.  $Q = \sqrt{\alpha G_N} M$  [30]. Where  $\alpha = \frac{G-G_N}{G_N}$  should be measured deviation of MOG from GR. Using this criterion the MOG action is given by

$$\mathcal{I}_{MOG} = \frac{1}{16\pi G} \int \sqrt{-g} R d^4x - \frac{1}{16\pi} \int \sqrt{-g} B_{ab} B^{ab} d^4x + \mathcal{I}_M \quad (2)$$

where  $R$  is the Ricci scalar,  $B_{ab}$  is the generalized field strength tensor of the vector field  $\phi^a$ ,  $B_{ab} = \partial_a \phi_b - \partial_b \phi_a$  and  $\mathcal{I}_M$  is the matter action.

The MOG field equations for vanishing matter electro-magnetic tensor  $\mathcal{T}_{Mab} = 0$  are

$$R_{ab} = -8\pi G \mathcal{T}_{\phi ab} . \quad (3)$$

where

$$\mathcal{T}_{\phi ab} = -\frac{1}{4\pi} \left( B_a^c B_{bc} - \frac{1}{4} g_{ab} B^{ef} B_{ef} \right) . \quad (4)$$

Thus vacuum field equations are

$$\frac{1}{\sqrt{-g}} \partial_a \left( \sqrt{-g} B^{ab} \right) = 0 , \quad (5)$$

and

$$\nabla_a B_{bc} + \nabla_b B_{ca} + \nabla_c B_{ab} = 0 . \quad (6)$$

where  $\nabla_a$  denotes covariant derivative with respect to the metric tensor  $g_{ab}$ . Using these criterion one obtains static spherical symmetric metric in MOG

$$ds^2 = \left[ 1 - \frac{2G_N(1+\alpha)M}{r} + \frac{G_N^2 M^2 \alpha(1+\alpha)}{r^2} \right] dt^2 - \frac{dr^2}{\left[ 1 - \frac{2G_N(1+\alpha)M}{r} + \frac{G_N^2 M^2 \alpha(1+\alpha)}{r^2} \right]} - r^2 d\Omega^2 . \quad (7)$$

where  $G_N$  is modified Newtonian constant which is related to the Newton's constant by  $G = G_N(1+\alpha)$  and modified charge parameter is  $Q = \sqrt{\alpha G_N} M$ , where  $\alpha$  is a MOG parameter. The above metric can be obtained by substituting these values in usual Reissner-Nordström BH solution. The metric of the rotating BH solution in MOG depends on the spin parameter  $a = J/M$ , where  $J$  is the Komar angular momentum of the asymptotically flat, axisymmetric, stationary spacetime. By applying Boyer-Lindquist coordinates one obtains the metric form which is written in Eq. (30) and it is quite similar structure of Kerr-Newman BH.

One of the main goals of this work is to explore the difference between BH and NS via computation of generalized spin frequency in MOG. For NS, the motivation comes from the works [23, 36, 37, 38, 39, 40, 41, 42]. How to differentiate a BH from a NS, this is a prime aim of the present work. What is a NS? A NS is a type of gravitational singularity without an event horizon. Whereas a BH is a type of gravitational compact object having an event horizon. Although the thermodynamic properties of BH is an established subject but the thermodynamics of NS is completely unknown [40]. Recently,

the image of a BH has been observed in EHT telescope [7] while for NS there is no evidence could be seen till date.

However in the present work, we would like to provide a detailed analysis of inertial frame dragging effect for *non-extremal situation*, *extremal situation* and *NS* in KMOG BH. Earlier mentioned that the KMOG BH is a new class of spinning BH proposed by Moffat [25] and it is constructed by the ADM mass parameter ( $\mathcal{M}$ ), spin parameter ( $a$ ) and a deformation parameter or MOG parameter ( $\alpha$ ) in comparison to Kerr BH which is defined only by the ADM mass parameter and the spin parameter.

First, we derive the generalized spin precession of a test gyroscope around the KMOG spacetime. Using this frequency, we differentiate the behavior of three compact objects: non-extremal BH, extremal BH and NS. We point out a clear distinction between these three compact objects graphically. Moreover, this result is compared with Kerr BH. Using generalized spin frequency versus radial diagram, one can distinguish three compact objects for various spin limits. Also, we investigate the generalized spin frequency for various angular coordinate values i. e.  $\theta = 0$ ,  $\theta = \frac{\pi}{6}$ ,  $\theta = \frac{\pi}{4}$ ,  $\theta = \frac{\pi}{3}$  and  $\theta = \frac{\pi}{2}$ . Furthermore, we examine the generalized spin frequency for ring singularity. Lastly, we compare these results with the result of vanishing angular angular velocity  $\Omega = 0$ . This is exactly the LT frequency when the other frequencies are excluded. From the LT frequency vs. radial diagram, we show that the LT frequency is influenced by the MOG parameter. When  $\Omega = 0$ , we also analyze the LT frequency for angular values i.e.  $\theta = 0$ ,  $\theta = \frac{\pi}{6}$ ,  $\theta = \frac{\pi}{4}$ ,  $\theta = \frac{\pi}{3}$  and  $\theta = \frac{\pi}{2}$ . Each diagram clearly exhibits the key difference between three compact objects.

Moreover, we compute three fundamental frequencies i.e. the Keplerian frequency ( $\Omega_\phi$ ), the radial epicyclic frequency ( $\Omega_r$ ) and the vertical epicyclic frequency ( $\Omega_\theta$ ). Using these frequencies we can find the difference between three compact objects. In [48], it was mentioned that the epicyclic frequencies are the main ingredients for the geodesic models of quasi-periodic-oscillations (QPO). Again these QPOs help us to testify the strong gravity in a novel way. The geodesic models were described by relativistic precession model (RPM) [49] and epicyclic resonance model (ERM) [50]. These models indicates that there exist low frequency (LF) QPO and twin high frequency (HF) QPO. From RPM, we can find that the upper and lower HF QPOs meets with the azimuthal frequency,  $\Omega_{per} = \Omega_\phi - \Omega_r$ . While the LF QPOs are computed by the nodal precession frequency,  $\Omega_{nod} = \Omega_\phi - \Omega_\theta$ . These three QPO frequencies ( $\Omega_\phi, \Omega_{per}, \Omega_{nod}$ ) could generate at the same orbital radius. Moreover these frequencies could serve as a tool in our investigation to study the crucial differences between three compact objects.

Furthermore, our technique suggests that a comparative study of stationary, axisymmetric KMOG spacetime for various values of spin parameter. The main findings of the present work is to highlight crucial differences between *non-extremal* KMOG BH, *extremal* KMOG BH and *NS* by using generalized spin precession frequency ( $\Omega_p$ ) and LT precession frequency ( $\Omega_{LT}$ ) of a test gyro. Also other frequencies like radial epicyclic frequency ( $\Omega_r$ ), vertical epicyclic frequency ( $\Omega_\theta$ ), Keplerian frequency ( $\Omega_\phi$ ), periastron precession frequency ( $\Omega_{per}$ ), nodal precession frequency ( $\Omega_{nod}$ ), the ratio  $\frac{\Omega_r}{\Omega_\phi}$ , the ratio  $\frac{\Omega_r}{\Omega_\theta}$  and the ratio  $\frac{\Omega_\theta}{\Omega_\phi}$  are also help us to support this result in strong gravity regime.

The paper is organized as follows: in sec. 2, we derive the generalized spin frequency in the background of KMOG spacetime for non-extremal, extremal and NS cases. A detailed study has been done and visualize the results for all cases. Using the spin frequency expression, we differentiate the non extremal BH, extremal BH and NS. Moreover in Sec. 3, we compute the LT frequency by using the result of generalized spin frequency where we have taken the value of angular frequency  $\Omega = 0$ . Also in the subsequent sub Sec., we have specialized the result for extremal spacetime. Furthermore, we study the accretion disk physics in Sec. 4, by deriving the epicyclic frequencies. We also derive the periastron frequency and nodal frequency. By using the frequency profile, we can distinguish three spacetimes namely the non-extremal spacetime, extremal spacetime and NS. In Sec. 5, we have discussed the result.

## 2 Generalized Spin precession of a test gyroscope around a stationary spacetime

In this section we shall provide the basic formalism (following the Ref. [43, 18]) of spin precession of a test gyroscope which is attached to a stationary observer and moves along a Killing path in a stationary spacetime with a timelike Killing vector field  $K$ . Then the spin of such a test gyroscope undergoes a Fermi-Walker transport along

$$u = \frac{K}{\sqrt{-K^2}}, \quad (8)$$

where  $K$  is the timelike Killing vector field. For a stationary observers, the four-velocity can be defined as  $u^\alpha = (u^t, 0, 0, \Omega u^t)$ . Where  $t$  is time coordinate and  $\Omega$  is the angular velocity of the observer. It is well-known that in the special case the frequency of the gyroscope may coincide with the vorticity field associated with the Killing congruence. This indicates that the said gyroscope is rotating with respect to a corotating frame along with an angular velocity. This effect is said to be a gravitomagnetic precession in gravitational physics because the vorticity vector behaves as the magnetic field in the  $3 + 1$  dimension spacetime [45]. Since our moto is to derive the spin precession frequency of a test gyroscope in a strong gravity regime hence the general spin precession frequency of a test gyro  $\Omega_s$  which is actually the rescaled vorticity field of the stationary observer can be derived as

$$\tilde{\Omega}_s = \frac{1}{2K^2} * (\tilde{K} \wedge d\tilde{K}) \quad (9)$$

or

$$(\Omega_s)_a = \frac{1}{2K^2} \eta_a{}^{bcd} K_b \partial_c K_d, \quad (10)$$

where  $\eta^{abcd}$  denotes the component of the volume-form in the spacetime,  $*$  denotes the Hodge dual, and  $\tilde{K}$  &  $\tilde{\Omega}_s$  represent the one-form of  $K$  &  $\Omega_s$ , respectively. The parameter  $\tilde{\Omega}_s$  will be vanish if and only if  $(\tilde{K} \wedge d\tilde{K})$  does vanish. This will be happen only in case of a static spacetime.

It has already been derived in [20, 21] the LT precession frequency of a test gyro due to the rotation of any stationary and axisymmetric spacetime

$$\vec{\Omega}_p|_{\Omega=0} = \frac{1}{2\sqrt{-g}} \times \left[ -\sqrt{g_{rr}} \left( g_{0\phi,\theta} - \frac{g_{0\phi}}{g_{00}} g_{00,\theta} \right) \hat{r} + \sqrt{g_{\theta\theta}} \left( g_{0\phi,r} - \frac{g_{0\phi}}{g_{00}} g_{00,r} \right) \hat{\theta} \right] \quad (11)$$

This result is valid for outside the ergoregion and  $\Omega = 0$ . For arbitrary value of  $\Omega$  the formalism is derived in Ref. [23]. The timelike Killing vector field in generalized spacetime can be written as

$$K = \partial_0 + \Omega \partial_s \quad (12)$$

where  $\partial_s$  is spacelike Killing vector of the said stationary spacetime and  $\Omega$  is angular velocity of an observer moving along integral curves of  $K$ . The metric of above stationary spacetime is independent of  $x^0$  and  $x^s$  coordinates. Thus the corresponding co-vector of  $K$  is

$$\tilde{K} = g_{0\alpha} dx^\alpha + \Omega g_{\beta s} dx^\beta, \quad (13)$$

where  $\beta, \alpha = 0, s, 2, 3$  in four dimension spacetime. Now one can write  $\tilde{K}$  by separating into space and time components as

$$\tilde{K} = (g_{00} dx^0 + g_{0s} dx^s + g_{0i} dx^i) + \Omega (g_{0s} dx^0 + g_{ss} dx^s + g_{is} dx^i) \quad (14)$$

where  $i = 2, 3$ . Since we are interested in ergoregion of the said stationary, axisymmetric spacetime thus we are neglecting the terms  $g_{0i}$  and  $g_{is}$  then one obtains

$$\tilde{K} = (g_{00} dx^0 + g_{0s} dx^s) + \Omega (g_{0s} dx^0 + g_{ss} dx^s) \quad (15)$$

and

$$d\tilde{K} = \left( g_{00,k} dx^k \wedge dx^0 + g_{0s,k} dx^k \wedge dx^s \right) + \Omega (g_{0s,k} dx^k \wedge dx^0 + g_{ss,k} dx^k \wedge dx^s). \quad (16)$$

Now, Eq. (10) can be re-written as

$$\tilde{\Omega}_p = \frac{1}{2K^2} * (\tilde{K} \wedge d\tilde{K}) \quad (17)$$

Substituting the values of  $\tilde{K}$  and  $d\tilde{K}$  in Eq. (17), one finds the one-form of the precession frequency

$$\tilde{\Omega}_p = \frac{\varepsilon_{skl} g_{l\mu} dx^\mu}{2\sqrt{-g} \left( 1 + 2\Omega \frac{g_{0s}}{g_{00}} + \Omega^2 \frac{g_{ss}}{g_{00}} \right)} \times$$

$$\left[ \left( g_{0s,k} - \frac{g_{0s}}{g_{00}} g_{00,k} \right) + \Omega \left( g_{ss,k} - \frac{g_{ss}}{g_{00}} g_{00,k} \right) + \Omega^2 \left( \frac{g_{0s}}{g_{00}} g_{ss,k} - \frac{g_{ss}}{g_{00}} g_{0s,k} \right) \right]$$

where we have used  $*(dx^0 \wedge dx^k \wedge dx^s) = \eta^{0ksl} g_{l\mu} dx^\mu = -\frac{1}{\sqrt{-g}} \varepsilon_{ksl} g_{l\mu} dx^\mu$  and  $K^2 = g_{00} + 2\Omega g_{0s} + \Omega^2 g_{ss}$ . The corresponding vector  $(\Omega_p)$  of the co-vector  $\tilde{\Omega}_p$  is

$$\Omega_p = \frac{\varepsilon_{skl}}{2\sqrt{-g} \left( 1 + 2\Omega \frac{g_{0s}}{g_{00}} + \Omega^2 \frac{g_{ss}}{g_{00}} \right)} \times$$

$$\left[ \left( g_{0s,k} - \frac{g_{0s}}{g_{00}} g_{00,k} \right) + \Omega \left( g_{ss,k} - \frac{g_{ss}}{g_{00}} g_{00,k} \right) + \Omega^2 \left( \frac{g_{0s}}{g_{00}} g_{ss,k} - \frac{g_{ss}}{g_{00}} g_{0s,k} \right) \right]$$

(18)

For a stationary and axisymmetric spacetime with coordinates  $t, r, \theta, \phi$ , the above equation becomes

$$\vec{\Omega}_p = \frac{-\sqrt{g_{rr}} \mathcal{X}(r) \hat{r} + \sqrt{g_{\theta\theta}} \mathcal{Y}(r) \hat{\theta}}{2\sqrt{-g} \mathcal{Z}(r)} \quad (19)$$

where

$$\mathcal{X}(r) = \mathcal{A} + \mathcal{B}\Omega + \mathcal{C}\Omega^2 \quad (20)$$

$$\mathcal{Y}(r) = \mathcal{F} + \mathcal{G}\Omega + \mathcal{H}\Omega^2 \quad (21)$$

$$\mathcal{Z}(r) = g_{tt} + 2g_{t\phi}\Omega + g_{\phi\phi}\Omega^2 \quad (22)$$

and

$$\mathcal{A} = g_{tt} g_{t\phi,\theta} - g_{t\phi} g_{tt,\theta} \quad (23)$$

$$\mathcal{B} = g_{tt} g_{\phi\phi,\theta} - g_{\phi\phi} g_{tt,\theta} \quad (24)$$

$$\mathcal{C} = g_{t\phi} g_{\phi\phi,\theta} - g_{\phi\phi} g_{t\phi,\theta} \quad (25)$$

$$\mathcal{F} = g_{tt} g_{t\phi,r} - g_{t\phi} g_{tt,r} \quad (26)$$

$$\mathcal{G} = g_{tt} g_{\phi\phi,r} - g_{\phi\phi} g_{tt,r} \quad (27)$$

$$\mathcal{H} = g_{t\phi} g_{\phi\phi,r} - g_{\phi\phi} g_{t\phi,r} \quad (28)$$

The most striking feature of Eq. (19) is that it could be applicable to derive the generalized spin precession for any stationary axisymmetric BH spacetime which is valid for both outside and inside the ergosphere. In the limit  $\Omega = 0$ , one obtains

$$\vec{\Omega}_{LT} = \frac{-\sqrt{g_{rr}} \mathcal{A} \hat{r} + \sqrt{g_{\theta\theta}} \mathcal{F} \hat{\theta}}{2\sqrt{-g} g_{tt}} \quad (29)$$

This formula is applicable only outside the ergoregion. This is the exact LT precession frequency of a test gyro due to rotation of any stationary and axisymmetric spacetime as mentioned in Eq. (11). It must be noted that  $\vec{\Omega}_p$  is not the  $\vec{\Omega}_{LT}$  of test gyro. Actually  $\vec{\Omega}_p$  describes the overall frequency of test gyro since gyro has non-zero angular velocity while  $\vec{\Omega}_{LT}$  describes LT frequency of test gyro when the test gyro has zero angular velocity i.e.  $\Omega = 0$ .



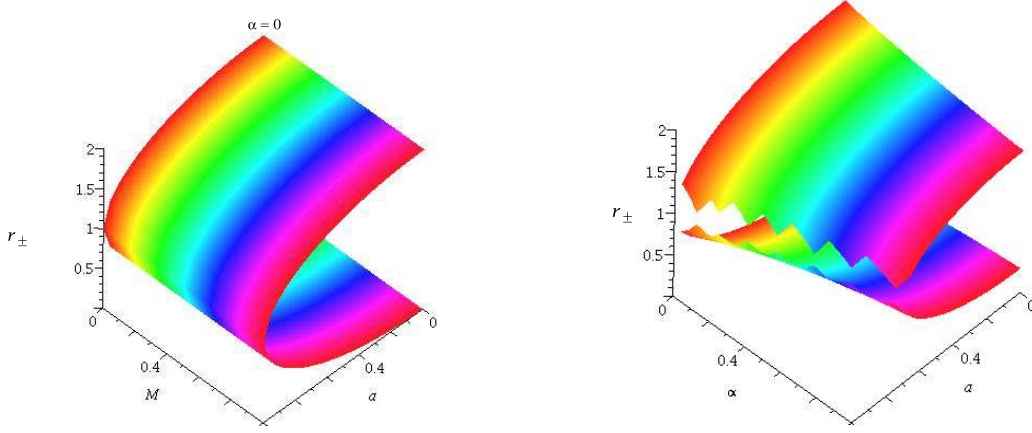


Figure 1: The figure implies the variation of  $r_{\pm}$  with  $a$  and  $\alpha$  for Kerr BH and Kerr-MOG BH. Left figure for Kerr BH. Right figure for Kerr-MOG BH. The presence of the MOG parameter is deformed the shape of the horizon radii.

## 2.1 Application to KMOG spacetime

In this subsection we will present a detailed analysis of the frame-dragging effect for KMOG spacetime according to the above formalism. To do this we have to write the metric explicitly for KMOG BH as described in Ref. [25]

$$ds^2 = -\frac{\Delta}{\rho^2} [dt - a \sin^2 \theta d\phi]^2 + \frac{\sin^2 \theta}{\rho^2} [(r^2 + a^2) d\phi - a dt]^2 + \rho^2 \left[ \frac{dr^2}{\Delta} + d\theta^2 \right] . \quad (30)$$

where

$$\begin{aligned} \rho^2 &\equiv r^2 + a^2 \cos^2 \theta \\ \Delta &\equiv r^2 - 2G_N(1 + \alpha)Mr + a^2 + G_N^2 \alpha(1 + \alpha)M^2 . \end{aligned} \quad (31)$$

where  $G_N$  is Newton's gravitational constant and  $M$  is Komar mass. We should mentioned that in the metric  $c = 1$ . The above metric is an axially-symmetric and stationary spacetime. The ADM mass and angular momentum are computed in [34] as  $\mathcal{M} = (1 + \alpha)M$  and  $J = a\mathcal{M}$ <sup>4</sup>. Substituting these values in Eq. (31) then  $\Delta$  becomes

$$\Delta = r^2 - 2G_N \mathcal{M}r + a^2 + \frac{\alpha}{1 + \alpha} G_N^2 \mathcal{M}^2 \quad (32)$$

The above metric describes a BH with horizon radii

$$r_{\pm} = G_N \mathcal{M} \pm \sqrt{\frac{G_N^2 \mathcal{M}^2}{1 + \alpha} - a^2} . \quad (33)$$

where  $r_+$  is called as event horizon and  $r_-$  is called as Cauchy horizon. Note that  $r_+ > r_-$ . The horizon structure could be seen visually in Fig. 1. It should be noted that when  $\alpha = 0$ , one gets the horizon radii of Kerr BH. The BH solution exists when  $\frac{G_N^2 \mathcal{M}^2}{1 + \alpha} > a^2$ . When  $\frac{G_N^2 \mathcal{M}^2}{1 + \alpha} = a^2$ , one obtains extremal BH. When  $\frac{G_N^2 \mathcal{M}^2}{1 + \alpha} < a^2$ , one gets the naked singularity case.

<sup>4</sup>One could determine the relation between the Komar mass and ADM mass as  $M = \frac{\mathcal{M}}{1 + \alpha}$ . If one could consider either the Komar mass or the ADM mass in the LT frequency computation then the physics will not be change. We consider here the ADM mass throughout the paper for our convenience.

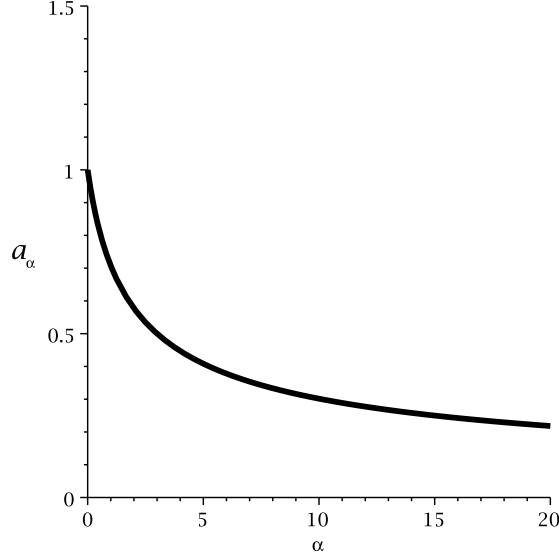


Figure 2: The figure indicates the variation of spin parameter  $a_\alpha$  with  $\alpha$ . Where  $a_\alpha = \frac{a}{G_N \mathcal{M}} = \frac{1}{\sqrt{1+\alpha}}$ . This means that the value of spin parameter decreases when MOG parameter increases. Maximum value of MOG parameter is unity. Its value gradually decreases when  $\alpha$  increases.

For the sake of convenience and to show the variation with deformation parameter we can define spin parameter for MOG BH as

$$a_\alpha = \frac{a}{G_N \mathcal{M}} = \frac{1}{\sqrt{1+\alpha}} \quad (34)$$

The new spin parameter  $a_\alpha$  varies with MOG parameter that could be seen from Fig. (2). From the plot we can infer that there is a restriction on spin parameter in MOG as

$$|a_\alpha| < \frac{1}{\sqrt{1+\alpha}} \quad \text{Non-extremal BH} \quad (35)$$

$$|a_\alpha| = \frac{1}{\sqrt{1+\alpha}} \quad \text{Extremal BH} \quad (36)$$

$$|a_\alpha| > \frac{1}{\sqrt{1+\alpha}} \quad \text{Naked Singularity} \quad (37)$$

Note that the MOG parameter or deformation parameter ( $\alpha$ ) is always positive definite. If we invert the above inequality then one gets the restriction on  $\alpha$ .

For a Kerr BH, when  $a_\alpha = \frac{a}{G_N \mathcal{M}} < 1$ , there exists a BH solution. While  $a_\alpha = \frac{a}{G_N \mathcal{M}} > 1$ , it is said to be a NS and  $a_\alpha = \frac{a}{G_N \mathcal{M}} = 1$  then it is said to be an extremal BH solution. While for a KMOG BH, these limits can be reduced in the following way. For example, if we take  $\alpha = 1$  then these limits are defined as  $a_\alpha = \frac{1}{\sqrt{2}} = 0.7$  which is the extremal limit,  $a_\alpha > \frac{1}{\sqrt{2}}$  is the NS situation and  $a_\alpha < \frac{1}{\sqrt{2}}$  is the BH solution. Similarly, if we take the MOG parameter  $\alpha = 2$ , then these limits are:  $a_\alpha = \frac{1}{\sqrt{3}}$  which is the extremal limit,  $a_\alpha > \frac{1}{\sqrt{3}}$  is the NS situation and  $a_\alpha < \frac{1}{\sqrt{3}}$  is the BH solution. The outer and inner ergosphere are occur at

$$r = r_e^\pm(\theta) = G_N \mathcal{M} \pm \sqrt{\frac{G_N^2 \mathcal{M}^2}{1+\alpha} - a^2 \cos^2 \theta}. \quad (38)$$

and they satisfied the following inequality  $r_e^-(\theta) \leq r_- \leq r_+ \leq r_e^+(\theta)$ . The structure of the outer and inner ergosphere could be seen visually from Fig. 3. In the extremal limit, the outer horizon and inner



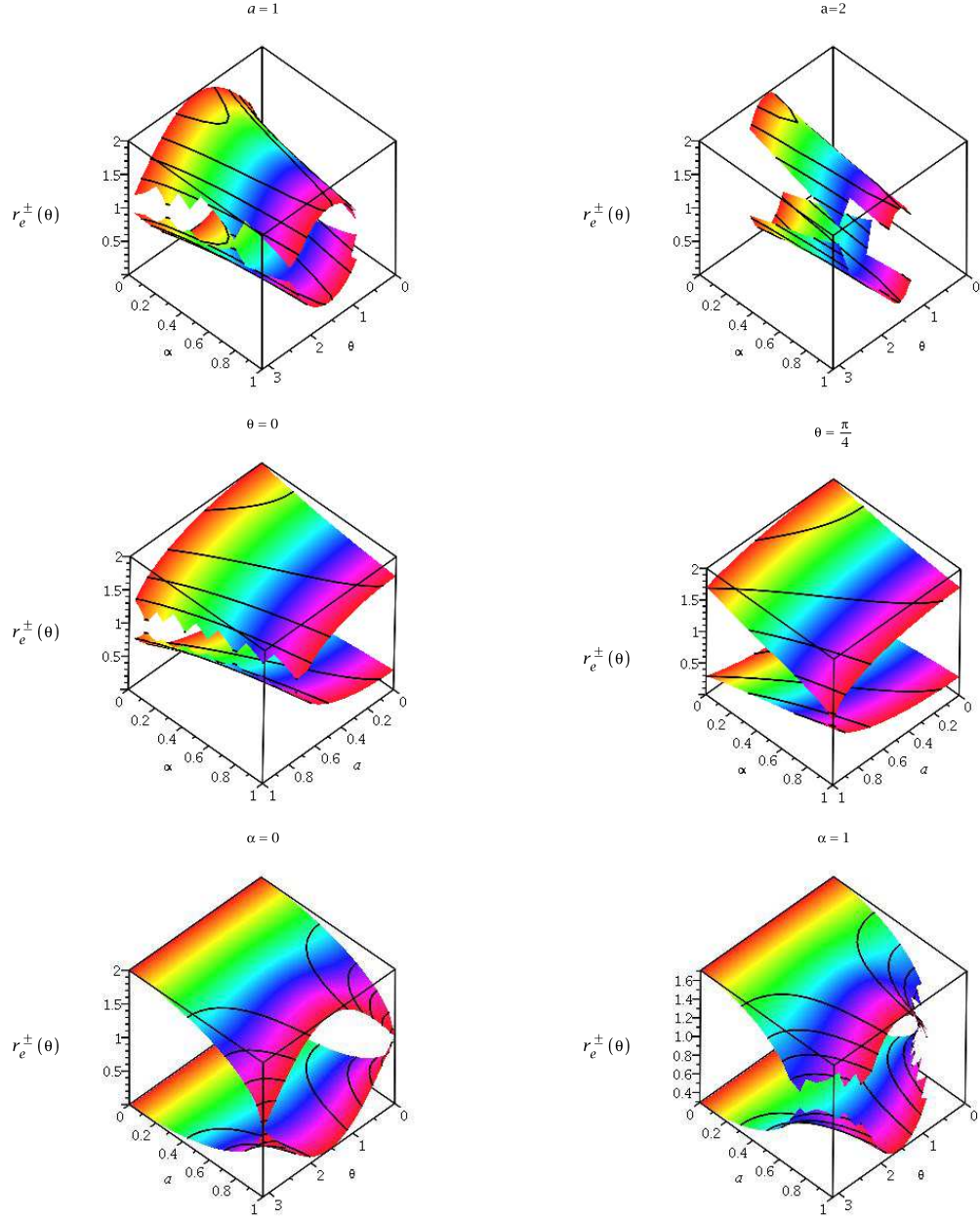


Figure 3: The figure indicates the variation of  $r_e^{\pm}(\theta)$  with  $a$  and  $\alpha$  for Kerr BH and Kerr-MOG BH. In each plot upper half corresponds to  $r_e^{+}(\theta)$  and lower half corresponds to  $r_e^{-}(\theta)$ .

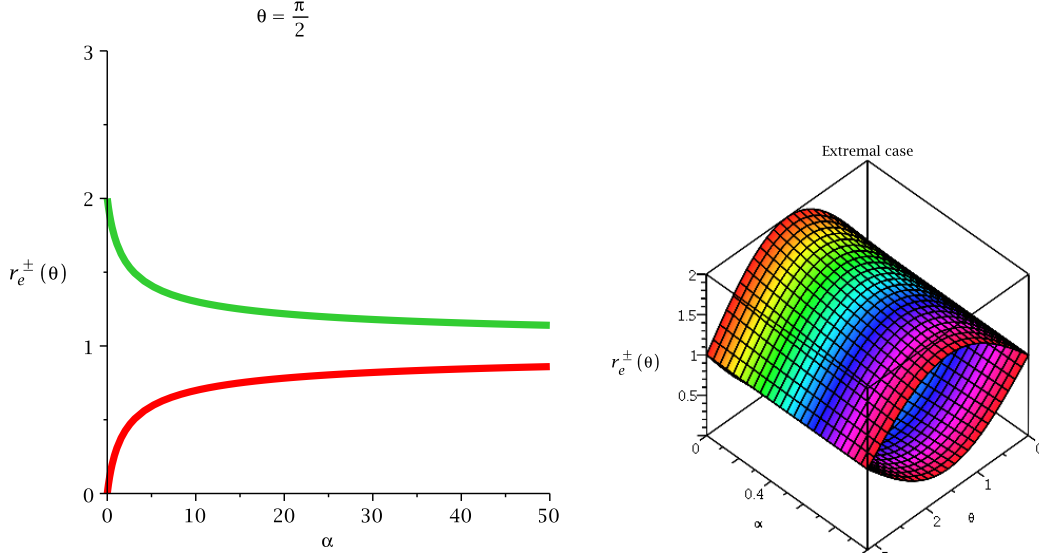


Figure 4: The figure implies the variation of  $r_e^\pm(\theta)$  with  $\alpha$  for extremal Kerr-MOG BH in equatorial plane.

horizon are coincident at  $r_+ = r_- = G_N \mathcal{M}$ . The outer and inner ergosphere radius reduces to

$$r_e^\pm(\theta) = G_N \mathcal{M} \left( 1 \pm \frac{\sin \theta}{\sqrt{1 + \alpha}} \right). \quad (39)$$

$$r_e^\pm(\theta)|_{\theta=0} = G_N \mathcal{M} = r_\pm, \quad (\text{on axis}) \quad (40)$$

$$r_e^\pm(\theta)|_{\theta=\frac{\pi}{2}} = G_N \mathcal{M} \left( 1 \pm \frac{1}{\sqrt{1 + \alpha}} \right) = r_\pm|_{a=0} \quad (\text{equatorial plane}). \quad (41)$$

The structure of the equatorial ergosphere could be seen visually from Fig. 4.

In the limit  $\alpha = 0$ ,

$$r_e^+(\theta)|_{\theta=\frac{\pi}{2}} = 2G_N \mathcal{M}, \quad r_e^-(\theta)|_{\theta=\frac{\pi}{2}} = 0. \quad (42)$$

This surface is outer to the event horizon or outer horizon and it coincides with the outer horizon at the poles  $\theta = 0$  and  $\theta = \pi$ . The metric components of above BH in Boyer-Lindquist coordinate are

$$g_{tt} = - \left( \frac{r^2 - \Pi_\alpha + a^2 \cos^2 \theta}{\rho^2} \right) \quad (43)$$

$$g_{t\phi} = - \left( \frac{a \sin^2 \theta \Pi_\alpha}{\rho^2} \right) \quad (44)$$

$$g_{rr} = \left( \frac{\rho^2}{\Delta} \right) \quad (45)$$

$$g_{\theta\theta} = \rho^2 \quad (46)$$

$$g_{\phi\phi} = \left( r^2 + a^2 + \frac{a \Pi_\alpha \sin^2 \theta}{\rho^2} \right) \sin^2 \theta \quad (47)$$

and

$$\sqrt{-g} = \rho^2 \sin \theta. \quad (48)$$

where

$$\Pi_\alpha = \left( 2G_N \mathcal{M} r - \frac{\alpha}{1 + \alpha} G_N^2 \mathcal{M}^2 \right) \quad (49)$$

Putting these metric components in Eq. (19), one obtains the generalized spin precession frequency of a test gyro for KMOG BH

$$\vec{\Omega}_p = \frac{\xi(r) \sqrt{\Delta} \cos \theta \hat{r} + \eta(r) \sin \theta \hat{\theta}}{\zeta(r)}, \quad (50)$$

where,

$$\begin{aligned} \xi(r) = & a\Pi_\alpha - \frac{\Omega}{8} [8r^4 + 8a^2r^2 + 8a^2\Pi_\alpha + 3a^4 + 4a^2(2\Delta - a^2)\cos 2\theta + a^4\cos 4\theta] \\ & + \Omega^2 a^3 \Pi_\alpha \sin^4 \theta \end{aligned} \quad (51)$$

$$\begin{aligned} \eta(r) = & aG_N\mathcal{M}(r^2 - a^2\cos^2\theta) - \frac{\alpha}{1+\alpha}G_N^2\mathcal{M}^2ar + \\ & \Omega(r^5 - 3G_N\mathcal{M}r^4 + 2a^2r^3\cos^2\theta - 2G_N\mathcal{M}a^2r^2 + a^4\cos^4\theta r) \\ & + \Omega \left[ G_N\mathcal{M}a^4\cos^2\theta(1 + \sin^2\theta) + 2\frac{\alpha}{1+\alpha}G_N^2\mathcal{M}^2r(r^2 + a^2) \right] \\ & + \Omega^2 G_N\mathcal{M}a\sin^2\theta [3r^4 + a^2r^2 + a^2\cos^2\theta(r^2 - a^2)] \\ & - \frac{\alpha}{1+\alpha}G_N^2\mathcal{M}^2a\sin^2\theta\Omega^2r [2r^2 + a^2(1 + \cos^2\theta)] \end{aligned} \quad (52)$$

$$\zeta(r) = \rho^3 [(\rho^2 - \Pi_\alpha) + 2a\Omega\Pi_\alpha\sin^2\theta - \Omega^2\sin^2\theta \{ \rho^2(r^2 + a^2) + a^2\Pi_\alpha\sin^2\theta \}] \quad (53)$$

This is the expression of generalized spin frequency which is valid both for outside and inside the ergosphere. Now we could determine the range of the angular velocity and therefore the four velocity must be time-like i.e.  $K^2 = g_{\phi\phi}\Omega^2 + 2g_{t\phi}\Omega + g_{tt} < 0$ . The allowed values of  $\Omega$  at any fixed  $(r, \theta)$  are  $\Omega_-(r, \theta) < \Omega(r, \theta) < \Omega_+(r, \theta)$  where

$$\Omega_\pm = \frac{-g_{t\phi} \pm \sqrt{g_{t\phi}^2 - g_{\phi\phi}g_{tt}}}{g_{\phi\phi}}. \quad (54)$$

For KMOG BH, it should be

$$\Omega_\pm = \frac{a\Pi_\alpha \sin \theta \pm \rho^2 \sqrt{\Delta}}{\sin \theta [\rho^2(r^2 + a^2) + a^2\Pi_\alpha \sin^2 \theta]} \quad (55)$$

Now we shall calculate the values of  $\Omega$  when an observer closes to the horizon. At the event horizon the angular velocity becomes  $\Omega_+ = \frac{a}{2G_N\mathcal{M}r_+ - \frac{\alpha}{1+\alpha}G_N^2\mathcal{M}^2}$  and at the Cauchy horizon the angular velocity becomes  $\Omega_- = \frac{a}{2G_N\mathcal{M}r_- - \frac{\alpha}{1+\alpha}G_N^2\mathcal{M}^2}$ . In the equatorial plane

$$\Omega_\pm|_{\theta=\pi/2} = \frac{a\Pi_\alpha \pm r^2\sqrt{\Delta}}{r^2(r^2 + a^2) + a^2\Pi_\alpha}. \quad (56)$$

Finally at the ring singularity  $r = 0$  and  $\theta = \frac{\pi}{2}$

$$\Omega_\pm|_{r=0, \theta=\pi/2} = 1. \quad (57)$$

This means that two angular frequencies coincide at the ring singularity. Variation of angular frequency ( $\Omega$ ) of a stationary gyroscope could be observed from the whale diagram[Figure (5)]. The significance of whale diagram is that the whale or a fish can move along the  $\Omega_+$  and  $\Omega_-$  and it is

prominent when the MOG parameter vanishes i.e.  $\alpha = 0$ . For details of whale diagram and escape cones one can see an interesting work by Tanatorov and Zaslavskii [52]. We set the value of  $\mathcal{M} = G_N = 1$  during plot which is valid throughout the work. In Fig. 5(a), Fig. 5(b) and Fig. 5(c), we also set the MOG parameter ( $\alpha = 0$ ) and will vary the spin parameter value to differentiate three types of compact objects namely non-extremal Kerr, extremal Kerr and NS. Three pictures are qualitatively different to differentiate between non-extremal BH, extremal BH and NS. In Fig. 5(d), Fig. 5(e) and Fig. 5(f), we set the value of MOG parameter is unity. In this case, one can see the variation of angular velocity with radial coordinate to differentiate three compact objects. Both  $\Omega_+$  and  $\Omega_-$  are clearly distinct in each case. The distinction is more pronounced in Fig. 5(g), Fig. 5(h) and Fig. 5(i) and so on for greater value of MOG parameter. The angular frequency has two values i. e. in the outer horizon it is  $\Omega_+$  and in the inner horizon it is  $\Omega_-$ . Now we analyze the behavior of the gyro inside the ergosphere of a BH and to do this job we should first compute the magnitude of the precession frequency for various values of  $\theta$ . For this purpose, we introduce the parameter  $\delta$  to scan the entire range of  $\Omega$  as

$$\Omega = \delta \Omega_+ + (1 - \delta) \Omega_- = \omega - (1 - 2\delta) \sqrt{\omega^2 - \frac{g_{tt}}{g_{\phi\phi}}} \quad (58)$$

$$= \frac{a \Pi_\alpha \sin \theta - (1 - 2\delta) \rho^2 \sqrt{\Delta}}{\sin \theta [(r^2 + a^2) \rho^2 + a^2 \sin^2 \theta \Pi_\alpha]} \quad (59)$$

where  $0 < \delta < 1$  and  $\omega = -g_{t\phi}/g_{\phi\phi}$ . It is evident that the limiting value of  $\delta$  gives the range of  $\Omega$  from  $\Omega_+$  to  $\Omega_-$ . Using Eq. (59), one obtains the generalized spin precession frequency in a compact form

$$\vec{\Omega}_p = \Upsilon(r) \left[ \xi(r) \sqrt{\Delta} \cos \theta \hat{r} + \eta(r) \sin \theta \hat{\theta} \right]. \quad (60)$$

where

$$\Upsilon(r) = \frac{(r^2 + a^2)^2 - a^2 \Delta \sin^2 \theta}{4\delta(1 - \delta)\Delta \rho^7} \quad (61)$$

The implication of this equation is that one could study the behaviour of generalized spin frequency  $\vec{\Omega}_p$  with spin parameter  $a$ ,  $\theta$ ,  $\delta$ ,  $r$  and MOG parameter. It should be noted that the frequency vector diverges at  $\delta = 0, 1$ ,  $\Delta = 0$  and  $\rho = 0$ . This means that the generalized spin precession frequency becomes arbitrarily large at these values. Using this frequency one should differentiate between the BH and NS in a strong gravitational field.

Now consider an observer moving with a four velocity  $u$  in a stationary and axisymmetric space-time. If the angular momentum is zero for a particular situation which is defined by

$$p_\phi \equiv \frac{\partial \mathcal{L}}{\partial \dot{\phi}} = g_{t\phi} \dot{t} + g_{\phi\phi} \dot{\phi} = \ell = 0. \quad (62)$$

(where  $\mathcal{L}$  is the Lagrangian and  $\ell$  is angular momentum) such an observer is called zero angular momentum observer (ZAMO) which was first observed by Bardeen [46, 53]. Bardeen et al. [47] proved that the ZAMO frame is a powerful tool to analyze the physical processes near astrophysical object. What happens in case of Newtonian gravity? The angular momentum  $\ell$  and angular velocity  $\Omega$  are satisfied by the relation  $\ell = r^2 \Omega$ . It implies that there is no problem when we taking into consider the non-rotating frame i.e.  $\ell = \Omega = 0$ . The problem should arise when we consider Einstein's gravity: in this case the angular momentum is satisfied the following relation  $\ell \propto (\Omega - \omega)$ , where  $\omega = -\frac{g_{t\phi}}{g_{\phi\phi}}$ . Here we would not obtain  $\ell = 0$  when  $\Omega = 0$ . It indicates that there must exist two different observers i.e. one should be zero angular momentum observer (ZAMO) and the other one should be zero angular velocity observer (ZAVO). In ZAMO frame, the value of angular momentum is  $\ell = 0$  while in ZAVO frame, the value of  $\Omega = 0$ . The frame-dragging angular velocity of these two frames is  $\omega = -\frac{g_{t\phi}}{g_{\phi\phi}}$ . One should define the gravitational potential in the ZAMO frame as  $\Phi = -\frac{1}{2} \ln |g^{tt}|$ . Where  $g^{tt}$

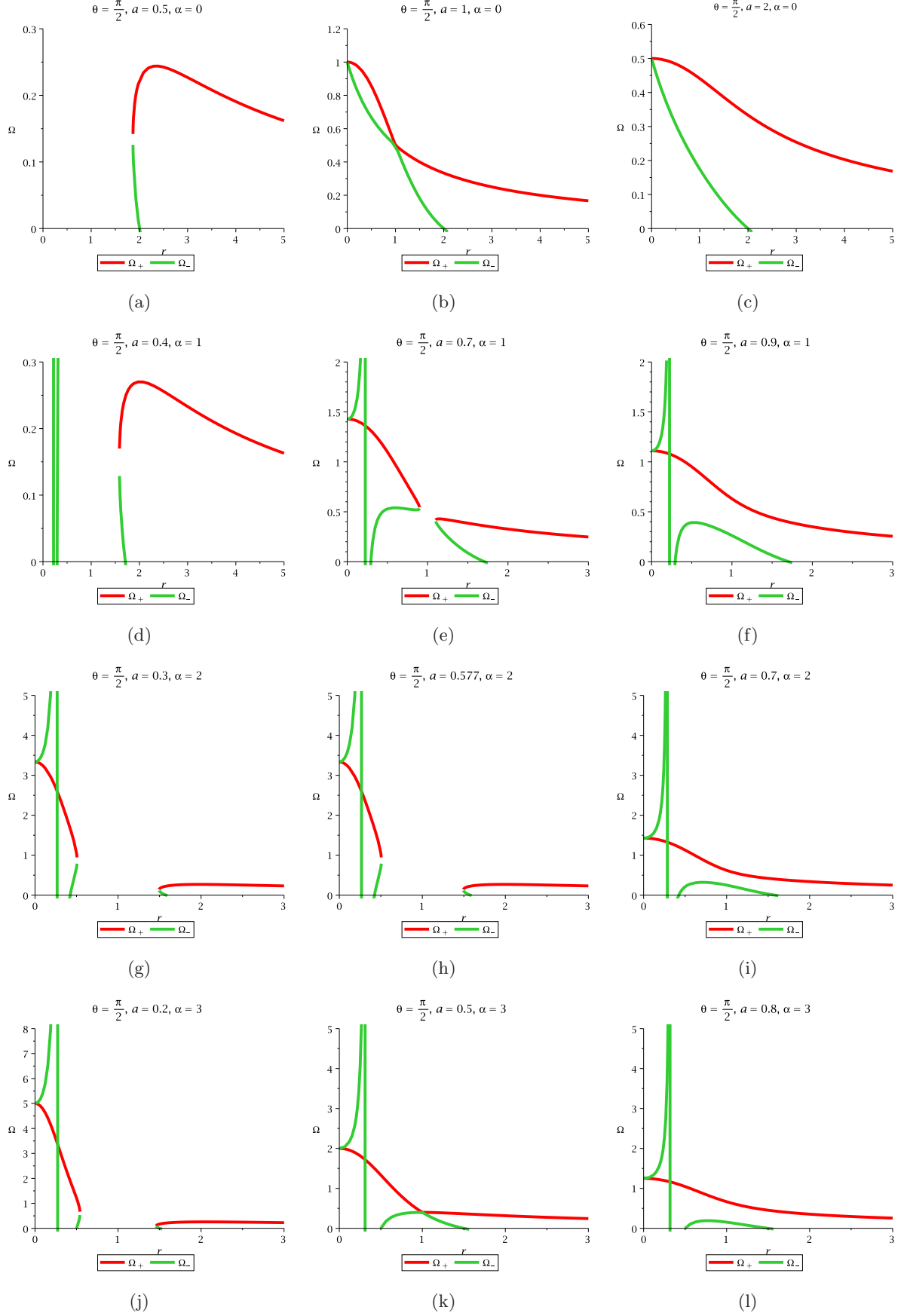


Figure 5: The figure describes the variation of  $\Omega$  with  $r$  for different values of spin parameter, with MOG parameter and without MOG parameter. The gyroscope has angular frequency  $\Omega$  varies with in the range  $(\Omega_+, \Omega_-)$ . Each set of row depicts the variation of  $\Omega$  vs.  $r$  for non-extremal BH, extremal BH and NS. There is a qualitative difference between these plots i. e. when we have taken into account the MOG parameter and without MOG parameter.

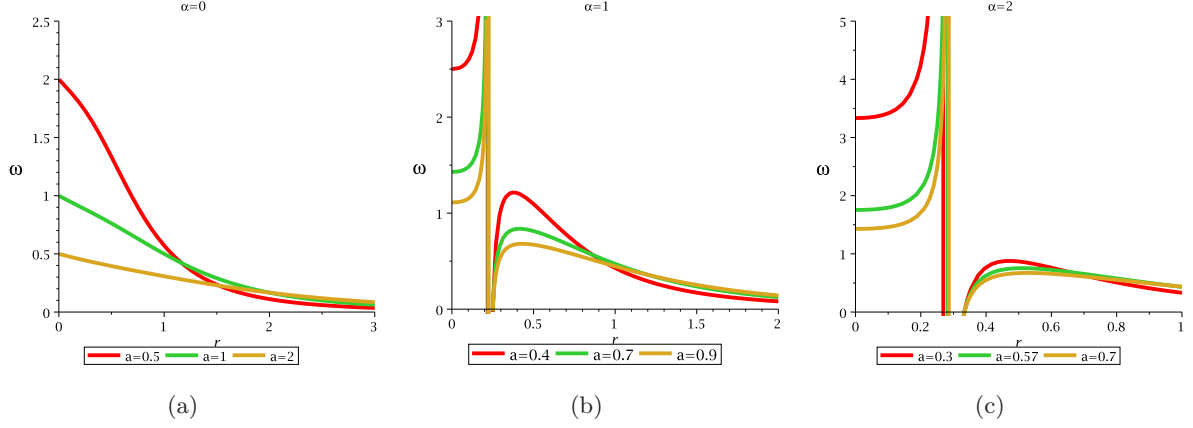


Figure 6: The figure depicts the variation of  $\omega$  with  $r$  for different values of spin parameter in  $\theta = \frac{\pi}{2}$  plane. This frequency is a special class of frequency called ZAMO frequency when  $\delta = \frac{1}{2}$ . The first figure is considered without MOG parameter ( $\alpha = 0$ ) and for various values of spin parameter to differentiate between non-extremal BH, extremal BH and NS. The second and third figure is considered with MOG parameter  $\alpha = 1$  and  $\alpha = 2$ . In first figure, the ZAMO frequency decreases for each spin values  $a < 1$ ,  $a = 1$  and  $a > 1$  for increasing the value of  $r$ . While in the second figure, the ZAMO frequency first increases then at certain point it diverges then it further increases to a certain peak then decreases (for each spin values).

is contravariant component of stationary axisymmetric spacetime metric. This potential is again related to the gravitational acceleration (acceleration due to gravity) as felt by an observer in space  $g_\mu = (a_\mu)_{ZAMO} = \nabla\Phi$ . The gravitational acceleration  $a_\mu$  is a kinematic invariant quantity. Using Eq. (59), one could easily see that for a particular value of  $\delta = \frac{1}{2}$  the value of angular velocity for KMOG BH in ZAMO frame as

$$\Omega = \omega = \frac{a \Pi_\alpha \sin \theta}{\sin \theta [(r^2 + a^2)\rho^2 + a^2 \sin^2 \theta \Pi_\alpha]} \quad (63)$$

It implies that the ZAMOs angular velocity is a function of spin parameter and charge parameter. In  $\theta = \frac{\pi}{2}$  plane, the ZAMOs angular velocity should be

$$\Omega|_{\theta=\frac{\pi}{2}} = \omega|_{\theta=\frac{\pi}{2}} = \frac{a \Pi_\alpha}{(r^2 + a^2)r^2 + a^2 \Pi_\alpha} \quad (64)$$

The variation of  $\Omega$  and  $\omega$  in the equatorial plane could be seen from Fig. (5) and Fig. (6) respectively. It must be noted that both these parameters are depend on MOG parameter. From Fig. (5) and Fig. (6), it is observed that the three cases namely non-extremal, extremal and NS both in the presence of MOG parameter and in the absence of MOG parameter are qualitatively different. This means that three geometries are quite distinguished.

## 2.2 Behaviour of $\vec{\Omega}_p$ at $r = 0$

In this section we will discuss various cases of LT precession frequency. Also we will see the LT precession frequency structure for various useful limits. First we have taken the limit  $r \rightarrow 0$  (i. e. at the ring singularity  $r = 0$ ,  $\theta = \frac{\pi}{2}$ ). It should be noted that  $\vec{\Omega}_p$  is not valid at the ring singularity ( $r = 0, \theta = \pi/2$ ). Yet, we should investigate its behavior in its vicinity i.e. in the region  $r = 0$ ,  $0 \leq \theta < 90^\circ$ . It must be noted that this region is completely outside the ergoregion since the ergosurface meets the ring singularity. At the  $r = 0$ , the LT precession frequency becomes

$$\vec{\Omega}_p|_{r=0} = \frac{\xi(\theta) \hat{r} + \eta(\theta) \hat{\theta}}{\zeta(\theta)}, \quad (65)$$



and the magnitude of this vector is thus

$$\Omega_p|_{r=0} = \frac{\sqrt{\xi^2(\theta) + \eta^2(\theta)}}{\zeta(\theta)} \quad (66)$$

where

$$\xi(\theta) = \sqrt{a^2 + \frac{\alpha}{1+\alpha} G_N^2 \mathcal{M}^2} \times$$

$$\left[ -\frac{\alpha}{1+\alpha} G_N^2 \mathcal{M}^2 - \frac{\Omega}{8} \left\{ (3 + 4 \cos 2\theta + \cos 4\theta) a^3 - 8 \frac{\alpha}{1+\alpha} G_N^2 \mathcal{M}^2 a (1 - \cos 2\theta) \right\} - \frac{\alpha}{1+\alpha} G_N^2 \mathcal{M}^2 a^2 \Omega^2 \sin^4 \theta \right] \quad (67)$$

$$\eta(\theta) = G_N \mathcal{M} a^2 \cos \theta \sin \theta [-1 + a\Omega(1 + \sin^2 \theta) - a^2 \Omega^2 \sin^2 \theta] \quad (68)$$

$$\zeta(\theta) = a^2 \cos^2 \theta \times$$

$$\left[ \frac{\alpha}{1+\alpha} G_N^2 \mathcal{M}^2 + a^2 \cos^2 \theta - 2 \frac{\alpha}{1+\alpha} G_N^2 \mathcal{M}^2 a \Omega \sin^2 \theta - a^2 \Omega^2 \sin^2 \theta \left( a^2 \cos^2 \theta - \frac{\alpha}{1+\alpha} G_N^2 \mathcal{M}^2 \sin^2 \theta \right) \right] \quad (69)$$

The valid regime of  $\Omega$  is

$$\Omega_-(\theta) < \Omega < \Omega_+(\theta) \quad (70)$$

where

$$\begin{aligned} \Omega_-(\theta) &= -\frac{\frac{\alpha}{1+\alpha} G_N^2 \mathcal{M}^2 \sin \theta + \sqrt{D}}{a \sin \theta \left[ a^2 - \left( a^2 + \frac{\alpha}{1+\alpha} G_N^2 \mathcal{M}^2 \right) \sin^2 \theta \right]} \\ \Omega_+(\theta) &= \frac{-\frac{\alpha}{1+\alpha} G_N^2 \mathcal{M}^2 \sin \theta + \sqrt{D}}{a \sin \theta \left[ a^2 - \left( a^2 + \frac{\alpha}{1+\alpha} G_N^2 \mathcal{M}^2 \right) \sin^2 \theta \right]} \end{aligned} \quad (71)$$

where

$$D = \left( \frac{\alpha}{1+\alpha} G_N^2 \mathcal{M}^2 \right)^2 \sin^2 \theta + \left\{ a^2 - \left( a^2 + \frac{\alpha}{1+\alpha} G_N^2 \mathcal{M}^2 \right) \sin^2 \theta \right\} \left( \frac{\alpha}{1+\alpha} G_N^2 \mathcal{M}^2 + a^2 \cos^2 \theta \right)$$

For a static observer outside the ergosphere we have to put  $\Omega = 0$  therefore we get from Eq. (65)

$$|\vec{\Omega}_p| = \frac{\sqrt{\left( \frac{\alpha}{1+\alpha} G_N^2 \mathcal{M}^2 \right)^2 \left( a^2 + \frac{\alpha}{1+\alpha} G_N^2 \mathcal{M}^2 \right) + \mathcal{M}^2 a^4 \sin^2 \theta \cos^2 \theta}}{a^2 \cos^2 \theta \left( \frac{\alpha}{1+\alpha} G_N^2 \mathcal{M}^2 + a^2 \cos^2 \theta \right)} \quad (72)$$

It must be noted that  $\Omega_p$  varies from  $0 \leq \Omega_p < \infty$  for  $0 \leq \theta < 90^\circ$  at  $r = 0$ . This indicates that it diverges only at the ring singularity and in cartesian Kerr-Schild coordinates it is described by  $x^2 + y^2 = a^2$ ,  $z = 0$  while it is finite inside the ring singularity i. e.  $x^2 + y^2 < a^2$ ,  $z = 0$ .

### 2.3 Behaviour of $\vec{\Omega}_p$ at $\theta = 0$

In the limit  $\theta = 0$ , the LT frequency is given by

$$\vec{\Omega}_p|_{\theta=0} = \frac{\xi(r)|_{\theta=0}}{\zeta(r)|_{\theta=0}} \sqrt{\Delta} \hat{r}, \quad (73)$$

where

$$\xi(r)|_{\theta=0} = a\Pi_\alpha - \frac{\Omega}{8} [8r^4 + 8a^2r^2 + 8a^2\Pi_\alpha + 3a^4 + 4a^2(2\Delta - a^2) + a^4] \quad (74)$$

$$\zeta(r)|_{\theta=0} = \rho^3 (\rho^2 - \Pi_\alpha) \quad (75)$$

Using the identity  $r^2 + a^2 - \Pi_\alpha = \Delta$ , the above equations reduced to

$$\xi(r)|_{\theta=0} = a\Pi_\alpha - \Omega (r^2 + a^2)^2 \quad (76)$$

$$\zeta(r)|_{\theta=0} = (r^2 + a^2)^{\frac{3}{2}} \Delta \quad (77)$$

The magnitude of this vector is calculated to be

$$\Omega_p|_{\theta=0} = \frac{a\Pi_\alpha - \Omega (r^2 + a^2)^2}{(r^2 + a^2)^{\frac{3}{2}} \sqrt{\Delta}} \quad (78)$$

From the above equation one could see that the precession frequency is arbitrarily large when  $\Delta = 0$ . The precession frequency is positive when  $a\Pi_\alpha > \Omega(r^2 + a^2)^2$  and negative when  $a\Pi_\alpha < \Omega(r^2 + a^2)^2$  and becomes zero when  $a\Pi_\alpha = \Omega(r^2 + a^2)^2$ . From Fig. (7), one could see that the variation of precession frequency with radial coordinate without MOG parameter and with MOG parameter. From this figure, one can distinguish three geometrical structure of the spacetime via precession frequency.

### 2.4 Behaviour of $\vec{\Omega}_p$ at $\theta = \frac{\pi}{6}$

In the limit  $\theta = \frac{\pi}{6}$ , the LT frequency is computed as

$$\vec{\Omega}_p|_{\theta=\frac{\pi}{6}} = \frac{\sqrt{3\Delta}\xi(r)|_{\theta=\frac{\pi}{6}}\hat{r} + \eta(r)|_{\theta=\frac{\pi}{6}}\hat{\theta}}{2\zeta(r)|_{\theta=\frac{\pi}{6}}}, \quad (79)$$

The magnitude of this vector is turned out to be

$$\Omega_p|_{\theta=\frac{\pi}{6}} = \frac{\sqrt{3\Delta\xi^2(r)|_{\theta=\frac{\pi}{6}} + \eta^2(r)|_{\theta=\frac{\pi}{6}}}}{2\zeta(r)|_{\theta=\frac{\pi}{6}}} \quad (80)$$

where

$$\xi(r)|_{\theta=\frac{\pi}{6}} = a\Pi_\alpha - \frac{\Omega}{16} (16r^4 + 24a^2r^2 + 8a^2\Pi_\alpha + 9a^4) + \frac{\Omega^2}{16} a^3\Pi_\alpha \quad (81)$$

$$\begin{aligned} \eta(r)|_{\theta=\frac{\pi}{6}} = & aG_N\mathcal{M} \left( r^2 - \frac{3}{4}a^2 \right) - \frac{\alpha}{1+\alpha} G_N^2\mathcal{M}^2 ar + \Omega \times \\ & \left[ r^5 - 3G_N\mathcal{M}r^4 + \frac{3}{2}a^2r^3 - 2G_N\mathcal{M}a^2r^2 + \frac{9}{16}a^4r + \frac{15}{16}G_N\mathcal{M}a^4 + \frac{2\alpha}{1+\alpha} G_N^2\mathcal{M}^2 r (r^2 + a^2) \right] \\ & + \frac{a\Omega^2}{4} \left[ G_N\mathcal{M} \left\{ 3r^4 + a^2r^2 + \frac{3}{4}a^2 (r^2 - a^2) \right\} - \frac{\alpha}{1+\alpha} G_N^2\mathcal{M}^2 r \left( 2r^2 + \frac{7}{4}a^2 \right) \right] \end{aligned} \quad (82)$$

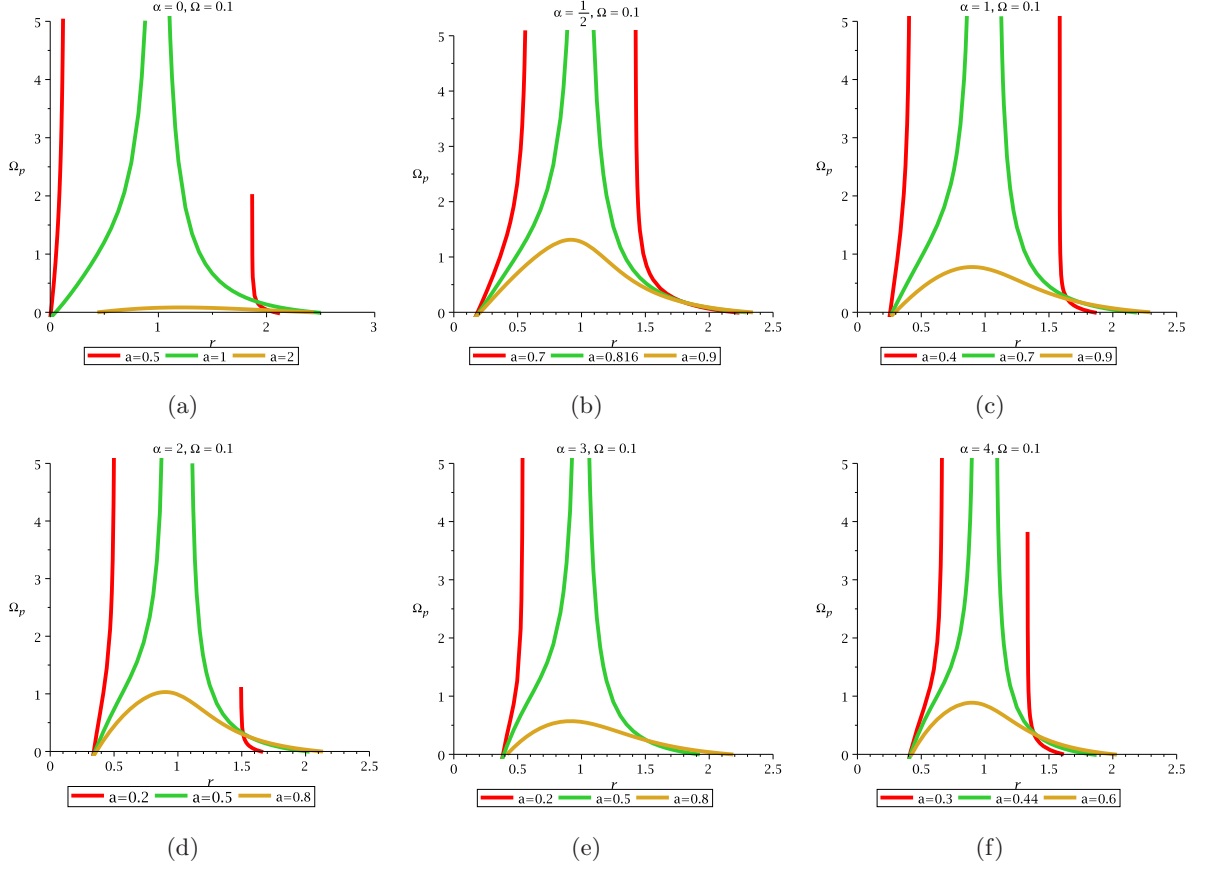


Figure 7: The figure describes the variation of precession frequency  $\Omega_p$  with  $r$  for  $\theta = 0$ . In this plot we have chosen the value of  $\Omega = 0.1$ . We have varied the spin parameter values for three cases namely non-extremal BH, extremal BH and NS. Each plot shows the difference between precession frequency  $\Omega_p$  having MOG parameter and without MOG parameter.

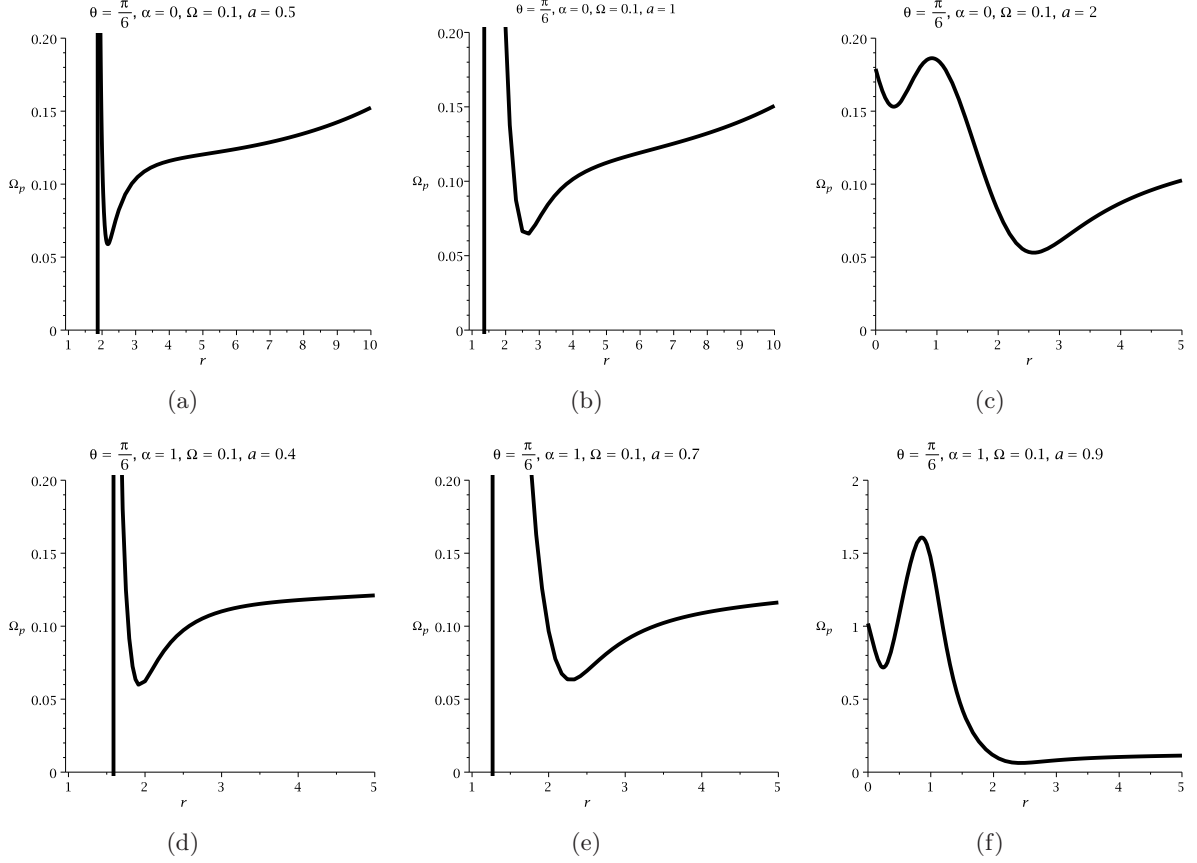


Figure 8: Examples of the variation of  $\Omega_p$  with  $r$  for  $\theta = \frac{\pi}{6}$  in KMOG with variation of MOG parameter, spin parameter and  $\Omega$ . The upper panel describes the variation of  $\Omega_p$  with  $r$  for non-extremal BH, extremal BH and NS without MOG parameter. The lower panel describes the variation of  $\Omega_p$  with  $r$  for non-extremal BH, extremal BH and NS with MOG parameter.

$$\zeta(r)|_{\theta=\frac{\pi}{6}} = \left(r^2 + \frac{3}{4}a^2\right)^{\frac{3}{2}} \times \left[ \left(r^2 + \frac{3}{4}a^2\right) - \Pi_\alpha + \frac{a\Omega\Pi_\alpha}{2} - \frac{\Omega^2}{4} \left\{ (r^2 + \frac{3}{4}a^2)(r^2 + a^2) + \frac{a^2\Pi_\alpha}{4} \right\} \right]. \quad (83)$$

Variation of spin precession frequency with radial coordinate with MOG parameter and without MOG parameter could be seen from Fig. (8). In Fig. (8-a), Fig. (8-b) and Fig. (8-c), we have plotted the precession frequency with radial variable for non-extremal BH, extremal BH and NS of Kerr spacetime. While in Fig. (8-d), Fig. (8-e) and Fig. (8-f), we have plotted the precession frequency for non-extremal BH, extremal BH and NS of KMOG spacetime. In upper panel [(8-a), Fig. (8-b), Fig. (8-c)], we can see that for BH spacetime the precession frequency has one minimum value while for NS it has two minima. In lower panel, [(8-d), Fig. (8-e), Fig. (8-f)], the generalized spin frequency has one minima for BH spacetime and one peak for NS.

## 2.5 Behaviour of $\vec{\Omega}_p$ at $\theta = \frac{\pi}{4}$

In the limit  $\theta = \frac{\pi}{4}$ , the LT frequency is derived as

$$\vec{\Omega}_p|_{\theta=\frac{\pi}{4}} = \frac{\sqrt{\Delta}\xi(r)|_{\theta=\frac{\pi}{4}}\hat{r} + \eta(r)|_{\theta=\frac{\pi}{4}}\hat{\theta}}{\sqrt{2}\zeta(r)|_{\theta=\frac{\pi}{4}}}, \quad (84)$$

The magnitude of this vector is

$$\Omega_p|_{\theta=\frac{\pi}{4}} = \frac{\sqrt{\Delta\xi^2(r)|_{\theta=\frac{\pi}{4}} + \eta^2(r)|_{\theta=\frac{\pi}{4}}}}{\sqrt{2}\zeta(r)|_{\theta=\frac{\pi}{4}}} \quad (85)$$

where

$$\xi(r)|_{\theta=\frac{\pi}{4}} = a\Pi_\alpha - \frac{\Omega}{8} [8r^4 + 8a^2r^2 + 8a^2\Pi_\alpha + 2a^4] + \frac{\Omega^2}{4}a^3\Pi_\alpha \quad (86)$$

$$\begin{aligned} \eta(r)|_{\theta=\frac{\pi}{4}} &= aG_N\mathcal{M} \left( r^2 - \frac{a^2}{2} \right) - \frac{\alpha}{1+\alpha}G_N^2\mathcal{M}^2ar + \frac{\Omega}{4} \times \\ &\left[ 4r^5 - 12G_N\mathcal{M}r^4 + 4a^2r^3 - 8G_N\mathcal{M}a^2r^2 + a^4r + 3G_N\mathcal{M}a^4 + \frac{8\alpha}{1+\alpha}G_N^2\mathcal{M}^2r(r^2 + a^2) \right] \\ &+ \frac{a\Omega^2}{4} \left[ G_N\mathcal{M}(6r^4 + 3a^2r^2 - a^4) - \frac{\alpha}{1+\alpha}G_N^2\mathcal{M}^2r(2r^2 + a^2) \right] \end{aligned} \quad (87)$$

$$\zeta(r)|_{\theta=\frac{\pi}{4}} = \left( r^2 + \frac{a^2}{2} \right)^{\frac{3}{2}} \times$$

$$\left[ \left( r^2 + \frac{a^2}{2} \right) - \Pi_\alpha + a\Omega\Pi_\alpha - \frac{\Omega^2}{2} \left\{ \left( r^2 + \frac{a^2}{2} \right) (r^2 + a^2) + \frac{a^2\Pi_\alpha}{2} \right\} \right]. \quad (88)$$

Variation of spin precession frequency with radial coordinate with MOG parameter and without MOG parameter may be seen from Fig. (9). In Fig. (9-a), Fig. (9-b) and Fig. (9-c), we have plotted the precession frequency with radial variable for non-extremal BH, extremal BH and NS of Kerr spacetime. While in Fig. (8-d), Fig. (8-e) and Fig. (8-f), we have plotted the precession frequency for non-extremal BH, extremal BH and NS of KMOG spacetime. In upper panel [(9-a), Fig. (9-b), Fig. (9-c)], one can see that for BH spacetime the precession frequency has one minimum value while for NS it has one minimum value and one maximum value. In lower panel, [(9-d), Fig. (9-e), Fig. (9-f)], the generalized spin frequency has one minima for BH spacetime and one peak for NS.

## 2.6 Behaviour of $\vec{\Omega}_p$ at $\theta = \frac{\pi}{3}$

In this limit  $\theta = \frac{\pi}{3}$ , the LT frequency is computed to be

$$\vec{\Omega}_p|_{\theta=\frac{\pi}{3}} = \frac{\sqrt{\Delta}\xi(r)|_{\theta=\frac{\pi}{3}}\hat{r} + \sqrt{3}\eta(r)|_{\theta=\frac{\pi}{3}}\hat{\theta}}{2\zeta(r)|_{\theta=\frac{\pi}{3}}}, \quad (89)$$

The magnitude of this vector is given by

$$\Omega_p|_{\theta=\frac{\pi}{3}} = \frac{\sqrt{\Delta\xi^2(r)|_{\theta=\frac{\pi}{3}} + 3\eta^2(r)|_{\theta=\frac{\pi}{3}}}}{2\zeta(r)|_{\theta=\frac{\pi}{3}}} \quad (90)$$

where

$$\xi(r)|_{\theta=\frac{\pi}{3}} = a\Pi_\alpha - \frac{\Omega}{8} \left( 8r^4 + 4a^2r^2 + 12a^2\Pi_\alpha + \frac{a^4}{2} \right) + \frac{9}{16}a^3\Omega^2\Pi_\alpha \quad (91)$$

$$\eta(r)|_{\theta=\frac{\pi}{3}} = aG_N\mathcal{M} \left( r^2 - \frac{a^2}{4} \right) - \frac{\alpha}{1+\alpha}G_N^2\mathcal{M}^2ar + \Omega \times$$

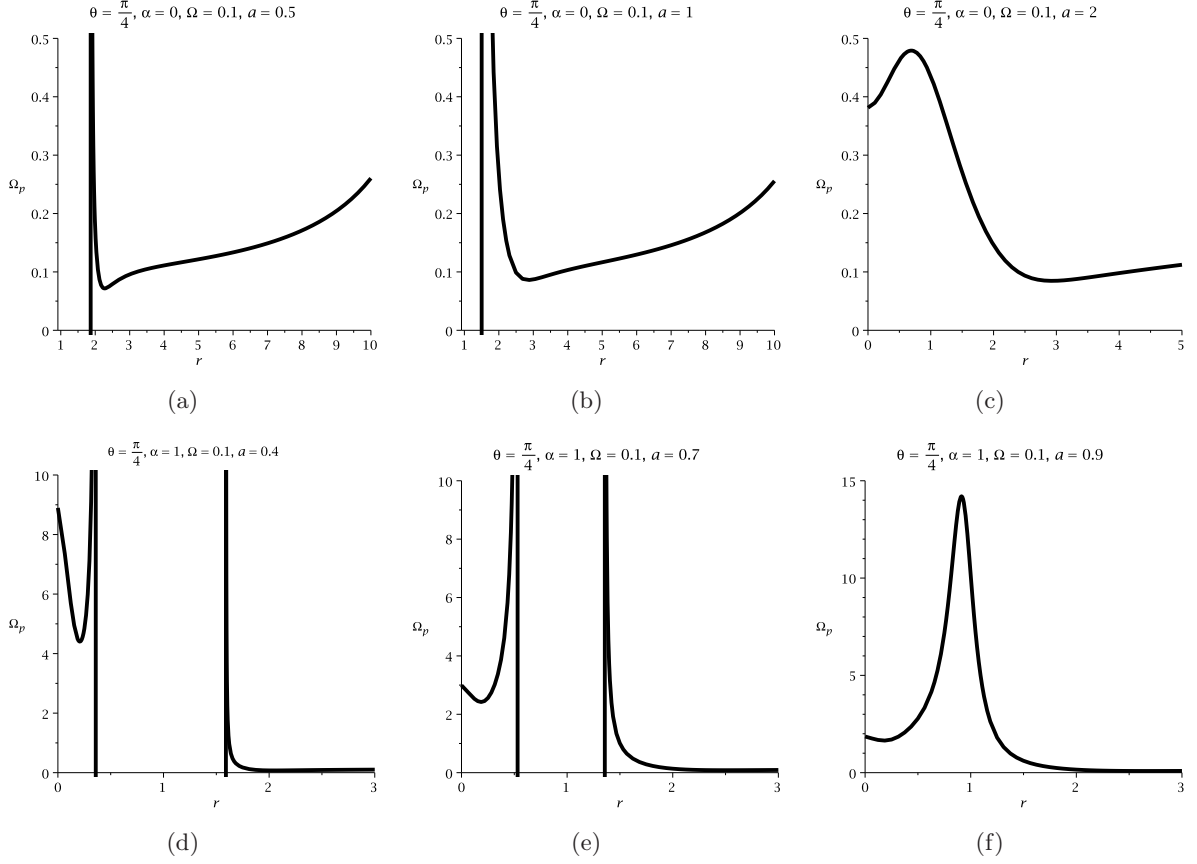


Figure 9: Examples of the variation of  $\Omega_p$  versus  $r$  for  $\theta = \frac{\pi}{4}$  in KMOG with variation of MOG parameter, spin parameter and  $\Omega$ . The first row describes the variation of  $\Omega_p$  with  $r$  for non-extremal BH, extremal BH and NS without MOG parameter. The second row describes the variation of  $\Omega_p$  with  $r$  for non-extremal BH, extremal BH and NS with MOG parameter.



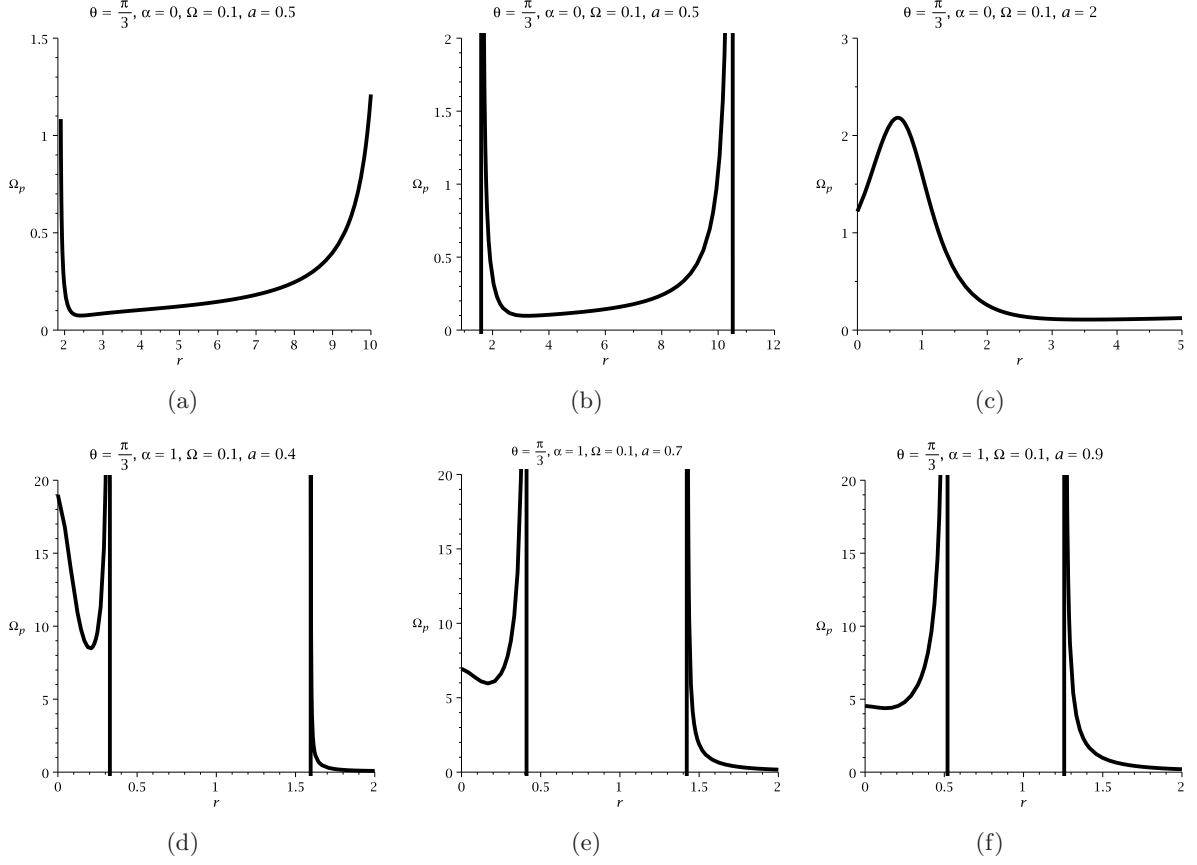


Figure 10: Examples of the variation of  $\Omega_p$  vs.  $r$  for  $\theta = \frac{\pi}{3}$  in KMOG with variation of MOG parameter, spin parameter and  $\Omega$ . The first row describes the variation of  $\Omega_p$  with  $r$  for non-extremal BH, extremal BH and NS without MOG parameter. The second row describes the variation of  $\Omega_p$  with  $r$  for non-extremal BH, extremal BH and NS with MOG parameter.

$$\begin{aligned}
& \left[ r^5 - 3G_N \mathcal{M} r^4 + \frac{a^2 r^3}{2} - 2G_N \mathcal{M} a^2 r^2 + \frac{a^4}{16} r + \frac{7}{16} G_N \mathcal{M} a^4 + \frac{2\alpha}{1+\alpha} G_N^2 \mathcal{M}^2 r (r^2 + a^2) \right] \\
& + \frac{3}{4} a \Omega^2 \left[ G_N \mathcal{M} \left( 3r^4 + a^2 r^2 + \frac{a^2}{4} (r^2 - a^2) \right) - \frac{\alpha}{1+\alpha} G_N^2 \mathcal{M}^2 r \left( 2r^2 + \frac{5}{4} a^2 \right) \right] \quad (92)
\end{aligned}$$

$$\zeta(r)|_{\theta=\frac{\pi}{3}} = \left( r^2 + \frac{a^2}{4} \right)^{\frac{3}{2}} \times$$

$$\left[ \left( r^2 + \frac{a^2}{4} \right) - \Pi_\alpha + \frac{3}{2} a \Omega \Pi_\alpha - \frac{3}{4} \Omega^2 \left\{ \left( r^2 + \frac{a^2}{4} \right) (r^2 + a^2) + \frac{3a^2 \Pi_\alpha}{4} \right\} \right]. \quad (93)$$

Analogously, the variation of spin precession frequency with radial coordinate with MOG parameter and without MOG parameter may be seen from Fig. (10).

## 2.7 Behaviour of $\vec{\Omega}_p$ at $\theta = \frac{\pi}{2}$

In the equatorial plane the precession frequency vector is given by

$$\vec{\Omega}_p|_{\theta=\frac{\pi}{2}} = \frac{\eta(r)|_{\theta=\frac{\pi}{2}}}{\zeta(r)|_{\theta=\frac{\pi}{2}}} \hat{\theta} \quad (94)$$

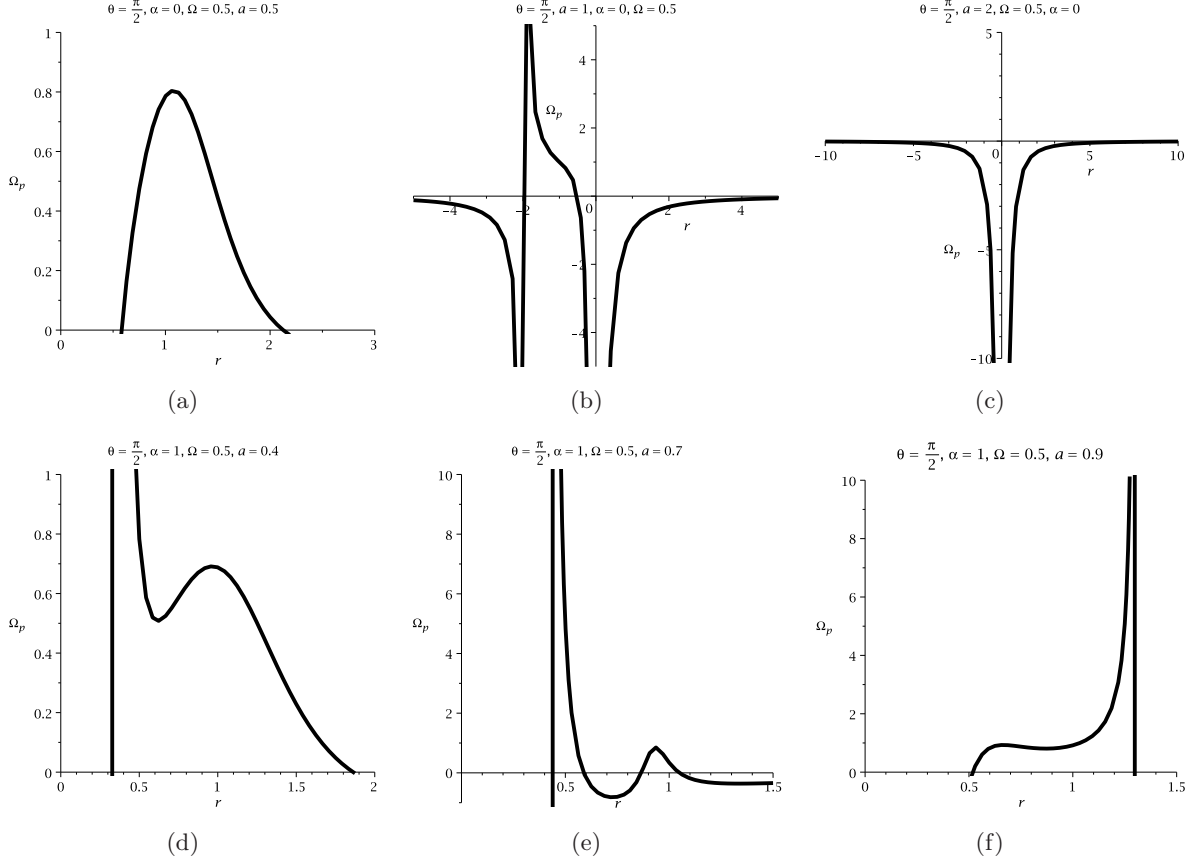


Figure 11: Examples of the variation of  $\Omega_p$  versus  $r$  for  $\theta = \frac{\pi}{2}$  in KMOG with variation of MOG parameter, spin parameter and  $\Omega$ . The first row describes the variation of  $\Omega_p$  with  $r$  for non-extremal BH, extremal BH and NS without MOG parameter. The second row describes the variation of  $\Omega_p$  with  $r$  for non-extremal BH, extremal BH and NS with MOG parameter.

The magnitude of this vector is thus

$$\Omega_p|_{\theta=\frac{\pi}{2}} = \frac{\eta(r)|_{\theta=\frac{\pi}{2}}}{\zeta(r)|_{\theta=\frac{\pi}{2}}} \quad (95)$$

where

$$\begin{aligned} \eta(r)_{\theta=\frac{\pi}{2}} &= ar \left( G_N \mathcal{M} r - \frac{\alpha}{1+\alpha} G_N^2 \mathcal{M}^2 \right) \\ &+ \Omega \left[ r^5 - 3G_N \mathcal{M} r^4 - 2G_N \mathcal{M} a^2 r^2 + 2 \frac{\alpha}{1+\alpha} G_N^2 \mathcal{M}^2 r (r^2 + a^2) \right] \\ &+ a \Omega^2 \left[ G_N \mathcal{M} r^2 (3r^2 + a^2) - \frac{\alpha}{1+\alpha} G_N^2 \mathcal{M}^2 r (2r^2 + a^2) \right] \end{aligned} \quad (96)$$

$$\zeta(r)_{\theta=\frac{\pi}{2}} = r^3 [r^2 - \Pi_\alpha + 2a\Omega\Pi_\alpha - \Omega^2 \{r^2 (r^2 + a^2) + a^2\Pi_\alpha\}] \quad (97)$$

Variation of spin precession frequency with radial coordinate with MOG parameter and without MOG parameter may be seen from Fig. (11). The range of  $\Omega$  could be determined by using Eq. (56). As we said earlier that the outer horizon and the outer ergosurface are located at  $r_+ = G_N \mathcal{M} + \sqrt{\frac{G_N^2 \mathcal{M}^2}{1+\alpha} - a^2}$  and  $r_e^+ = G_N \mathcal{M} + \sqrt{\frac{G_N^2 \mathcal{M}^2}{1+\alpha} - a^2 \cos^2 \theta}$ . While in the equatorial plane, the ergosphere is located at  $r_e^+ = m + \epsilon$  where  $m = G_N \mathcal{M}$  and  $\epsilon = \frac{m}{\sqrt{1+\alpha}}$ . Therefore one could obtain the precession frequency at

the equatorial ergosurface  $r = r_e^+ = m + \epsilon$

$$\Omega_p|_{r=r_e^+} = \frac{\eta(r)|_{r=r_e^+}}{\zeta(r)|_{r=r_e^+}} \quad (98)$$

where

$$\eta(r)|_{r=r_e^+} = (m + \epsilon) [am_\epsilon + \Omega m_{\epsilon\epsilon} + a\Omega^2 m_{\epsilon\epsilon\epsilon}] \quad (99)$$

where

$$\begin{aligned} m_\epsilon &= m^2 + m\epsilon - \alpha\epsilon^2 \\ m_{\epsilon\epsilon} &= (m + \epsilon)^2(\epsilon^2 - m\epsilon - 2m^2 + 2\alpha\epsilon^2) - 2ma^2(m + \epsilon) + 2\alpha\epsilon^2 a^2 \\ m_{\epsilon\epsilon\epsilon} &= 3m(m + \epsilon)^3 - 2\alpha\epsilon^2(m + \epsilon)^2 + ma^2(m + \epsilon) - \alpha\epsilon^2 a^2 \end{aligned}$$

and

$$\zeta(r)|_{r=r_e^+} = (m + \epsilon)^3 [m_\chi + 2a\Omega m_{\chi\chi} - \Omega^2 m_{\chi\chi\chi}] \quad (100)$$

where

$$\begin{aligned} m_\chi &= (1 + \alpha)\epsilon^2 - m^2 \\ m_{\chi\chi} &= 2m(m + \epsilon) - \alpha\epsilon^2 \\ m_{\chi\chi\chi} &= (m + \epsilon)^4 + a^2(m + \epsilon)^2 + 2ma^2(m + \epsilon) - \alpha\epsilon^2 a^2 \end{aligned}$$

In the extremal limit  $a = \epsilon$ , the precession frequency becomes

$$\Omega_p|_{\theta=\frac{\pi}{2}}^{r=r_e^+} = \frac{\epsilon [\epsilon - \Omega(3\epsilon^2 + 2\epsilon m + m^2) + \Omega^2(\epsilon^3 + m^3 + 4\epsilon m^2 + 7m\epsilon^2)]}{(\epsilon + m)^3 [2\epsilon\Omega - \Omega^2(3\epsilon^2 + m^2 + 2\epsilon m)]} \quad (101)$$

The value of  $\Omega$  lies in the range  $0 < \Omega < \frac{2\epsilon}{3\epsilon^2 + m^2 + 2\epsilon m}$ . It indicates that if the mass or angular momentum of the central object increases then the value of  $\Omega$  both at the ergosurface and in the  $\theta = \frac{\pi}{2}$  plane becomes decreases. It may be written as in terms of MOG parameter as

$$\begin{aligned} \Omega_p|_{\theta=\frac{\pi}{2}}^{r=r_e^+} &= \frac{1 + \alpha}{(1 + \sqrt{1 + \alpha})^3} \times \\ &\frac{1 - G_N \mathcal{M} \Omega \left( 2 + \sqrt{1 + \alpha} + \frac{3}{\sqrt{1 + \alpha}} \right) + G_N^2 \mathcal{M}^2 \Omega^2 \left( 4 + \sqrt{1 + \alpha} + \frac{7}{\sqrt{1 + \alpha}} + \frac{1}{1 + \alpha} \right)}{G_N^2 \mathcal{M}^2 \Omega \left[ 2 - G_N \mathcal{M} \Omega \left( 2 + \sqrt{1 + \alpha} + \frac{3}{\sqrt{1 + \alpha}} \right) \right]} \end{aligned} \quad (102)$$

when the MOG parameter reduces to zero value one gets the result of extremal Kerr BH as  $\Omega_p|_{\theta=\frac{\pi}{2}}^{r=r_e^+} = \frac{1 - 6G_N \mathcal{M} \Omega + 13G_N^2 \mathcal{M}^2 \Omega^2}{16G_N^2 \mathcal{M}^2 \Omega (1 - 3G_N \mathcal{M} \Omega)}$ . One could observe the variation of precession frequency with MOG parameter in the equatorial ergosphere from the Fig. (12). It should be noted that the precession frequency at the outer horizon  $r = r_+ = m$  of extremal KMOG BH is computed to be

$$\Omega_p|_{\theta=\frac{\pi}{2}}^{r=r_+} = -\frac{\epsilon}{m^2} \quad (103)$$

In terms of MOG parameter the above expression can be written as

$$\Omega_p|_{\theta=\frac{\pi}{2}}^{r=r_+} = -\frac{1}{\sqrt{1 + \alpha} G_N \mathcal{M}} \quad (104)$$

when  $\alpha = 0$ , the precession frequency reduces to extremal BH,  $\Omega_p|_{\theta=\frac{\pi}{2}}^{r=r_+} = -\frac{1}{G_N \mathcal{M}}$ .

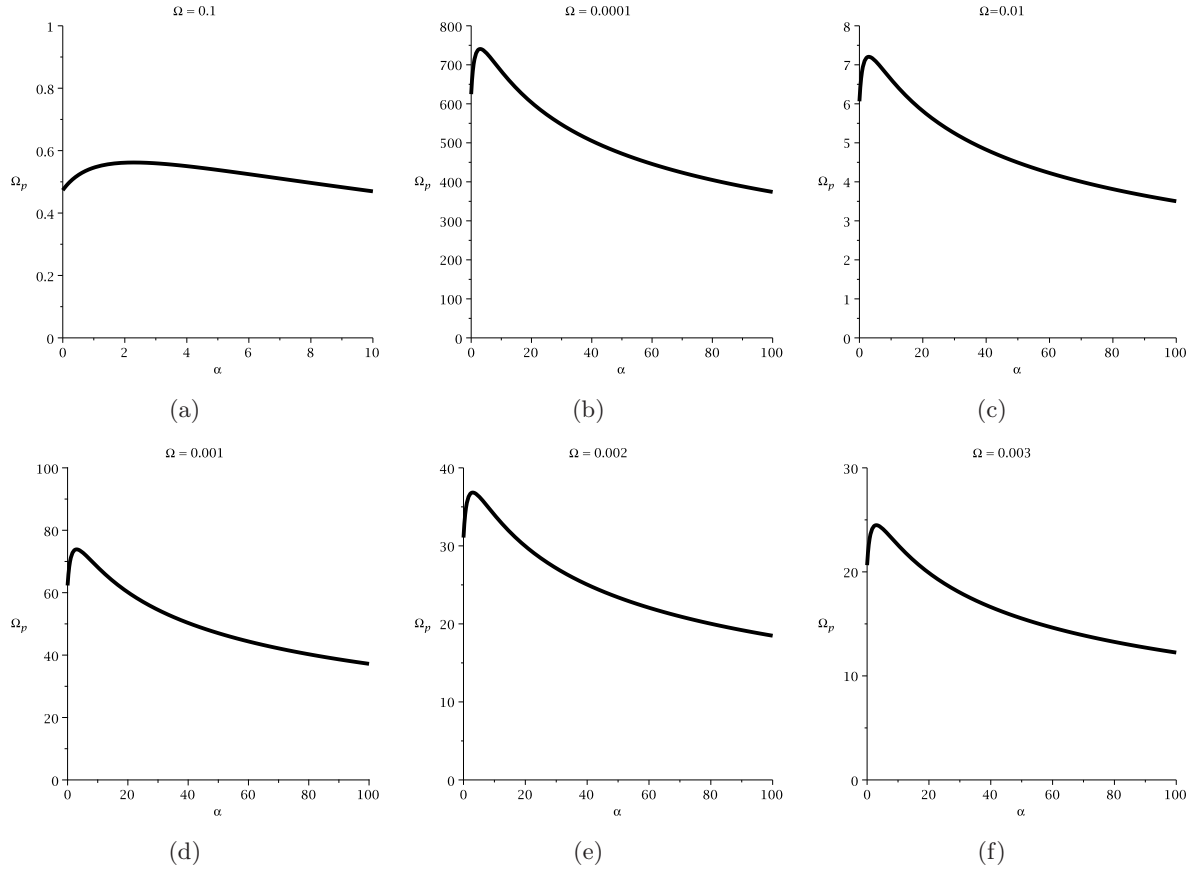


Figure 12: The figure describes the variation of  $\Omega_p$  with MOG parameter ( $\alpha$ ) for various values of  $\Omega$ .

## 2.8 $\vec{\Omega}_p$ in the Schwarzschild-MOG spacetime

In the limit  $a = 0$ , the KMOG BH reduces to Schwarzschild-MOG (SMOG) spacetime. In this case, the LT precession frequency becomes

$$\vec{\Omega}_p|_{a=0} = \Omega \frac{-(r^2 - \Pi_\alpha)^{\frac{1}{2}} \cos \theta \hat{r} + (r^2 - \Pi_\alpha - G_N \mathcal{M}r + \frac{\alpha}{1+\alpha} G_N^2 \mathcal{M}^2) \sin \theta \hat{\theta}}{r^2 - \Pi_\alpha - r^4 \Omega^2 \sin^2 \theta} \quad (105)$$

where  $\Omega$  might have any value so that  $u$  should be timelike.

It must be noted that SMOG spacetime is a spherically symmetric solution of the Einstein equation. It denotes a BH of mass  $\mathcal{M}$ . In the equatorial plane  $\Omega_p|_{\theta=\frac{\pi}{2}}$  becomes

$$\Omega_p = \Omega \frac{r^2 - \Pi_\alpha - G_N \mathcal{M}r + \frac{\alpha}{1+\alpha} G_N^2 \mathcal{M}^2}{r^2 - \Pi_\alpha - \Omega^2 r^4}. \quad (106)$$

It implies that when a gyroscope moving in the equatorial plane of the Reissner-Nordström spacetime (static spacetime) it becomes precess. Now if the gyro moves along circular orbits then  $\Omega_p$  becomes Keplerian frequency i.e.

$$\Omega_p = \Omega = \Omega_K = \sqrt{\frac{G_N \mathcal{M}r - \frac{\alpha}{1+\alpha} G_N^2 \mathcal{M}^2}{r^4}}. \quad (107)$$

This equation indicates the precession frequency in the Copernican frame which is derived with respect to the proper time  $\tau$ . The proper time  $\tau$  is computed in the Copernican frame is related to the coordinate frame  $t$  via the relation  $d\tau = \sqrt{1 - \frac{3G_N \mathcal{M}}{r} + 2\left(\frac{\alpha}{1+\alpha}\right) \frac{G_N^2 \mathcal{M}^2}{r^2}} dt$ . Thus one obtains the precession frequency in the coordinate basis  $\Omega'$  as,

$$\Omega' = \left( \frac{G_N \mathcal{M}r - \frac{\alpha}{1+\alpha} G_N^2 \mathcal{M}^2}{r^4} \right)^{\frac{1}{2}} \sqrt{1 - \frac{3G_N \mathcal{M}}{r} + 2\left(\frac{\alpha}{1+\alpha}\right) \frac{G_N^2 \mathcal{M}^2}{r^2}}. \quad (108)$$

Thus one can compute the geodetic precession frequency which is the difference between  $\Omega'$  and  $\Omega$ , and one obtains

$$\Omega_{\text{geodetic}} = \left( \frac{G_N \mathcal{M}r - \frac{\alpha}{1+\alpha} G_N^2 \mathcal{M}^2}{r^4} \right)^{\frac{1}{2}} \left( 1 - \sqrt{1 - \frac{3G_N \mathcal{M}}{r} + 2\left(\frac{\alpha}{1+\alpha}\right) \frac{G_N^2 \mathcal{M}^2}{r^2}} \right) \quad (109)$$

This is called the geodetic precession of a test gyroscope around a nonrotating spherical object of mass  $G_N \mathcal{M}$ . In the limit when  $\alpha = 0$ , one gets the geodetic precession of Schwarzschild BH [51]. One could see the geodetic precession of a nonrotating spherical object from the Fig. (13) for different values of MOG parameter.

## 3 Frame-Dragging effect of KMOG spacetime with $\Omega = 0$

For strengthening our work, in this section now we will focus on particularly LT effect by calculating the frequency  $\Omega_{LT}$  and considering the angular velocity of test gyro is equal to zero i.e.  $\Omega = 0$  (We omit other precession e.g. geodetic precession etc.). The theoretical prescription of this formalism for  $\Omega = 0$  was first introduced by Chakraborty & Majumdar [17] in the strong gravity regime and for arbitrary value of  $\Omega$ . The result of the weak field limit of the LT frequency can be easily obtained from the general formalism. Therefore, one can derive the LT precession frequency for KMOG BH in MOG by using Eq. (29).

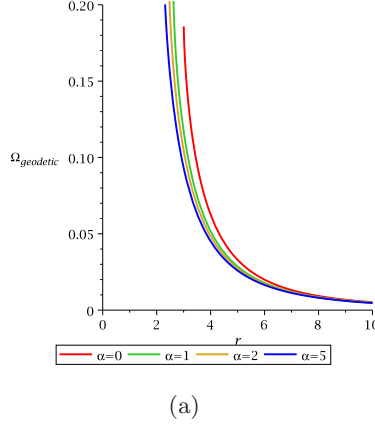


Figure 13: The figure describes the variation of geodetic precession with  $r$  for different values of spin parameter in the  $\theta = \frac{\pi}{2}$  plane.

As we have said earlier when  $\Omega = 0$  then  $\vec{\Omega}_p = \vec{\Omega}_{LT}$ . Thus one can compute for the metric (30) the LT frequency vector is

$$\vec{\Omega}_{LT} = \frac{\chi(r) \sqrt{\Delta} \cos \theta \hat{r} + \mu(r) \sin \theta \hat{\theta}}{\sigma(r)}, \quad (110)$$

where,

$$\begin{aligned} \chi(r) &= a\Pi_\alpha \\ \mu(r) &= aG_N \mathcal{M}(r^2 - a^2 \cos^2 \theta) - \frac{\alpha}{1+\alpha} G_N^2 \mathcal{M}^2 a r \\ \sigma(r) &= \rho^3 (\rho^2 - \Pi_\alpha) \end{aligned}$$

The magnitude of this vector is computed to be

$$\Omega_{LT}(r, \theta) = \frac{\sqrt{\Delta} \chi^2(r) \cos^2 \theta + \mu^2(r) \sin^2 \theta}{\sigma(r)} \quad (111)$$

It clearly shows that the LT frequency is affected by the MOG parameter  $\alpha$ . This is very interesting in a sense that the deformation parameter changes the geometry of the spacetime and it also changes the LT frequency. This could be seen from the graphical plot. Without MOG parameter the LT frequency reduces to Kerr BH. The presence of the MOG parameter decreases the LT frequency. Now we would derive the LT frequency for various values of  $\theta$ . One could see the variation of Lense-Thirring frequency with the radial coordinate from the subsequent figures. From this diagram one can observed how much amount of LT frequency is changed due to the deformation parameter.

### 3.1 Behaviour of $\vec{\Omega}_{LT}$ at $\theta = 0$

First we consider the case  $\theta = 0$ . In this case the LT frequency vector becomes

$$\vec{\Omega}_{LT}|_{\theta=0} = \frac{\chi(r)|_{\theta=0}}{\sigma(r)|_{\theta=0}} \sqrt{\Delta} \hat{r}, \quad (112)$$

The magnitude of this vector is calculated to be

$$\Omega_{LT}|_{\theta=0} = \frac{a\Pi_\alpha}{(r^2 + a^2)^{\frac{3}{2}} \sqrt{\Delta}} \quad (113)$$

It follows that the LT frequency depends on the MOG parameter. Using this equation one can differentiate between BHs and NS in MOG theory. It could be observed from the Fig. 14. In this



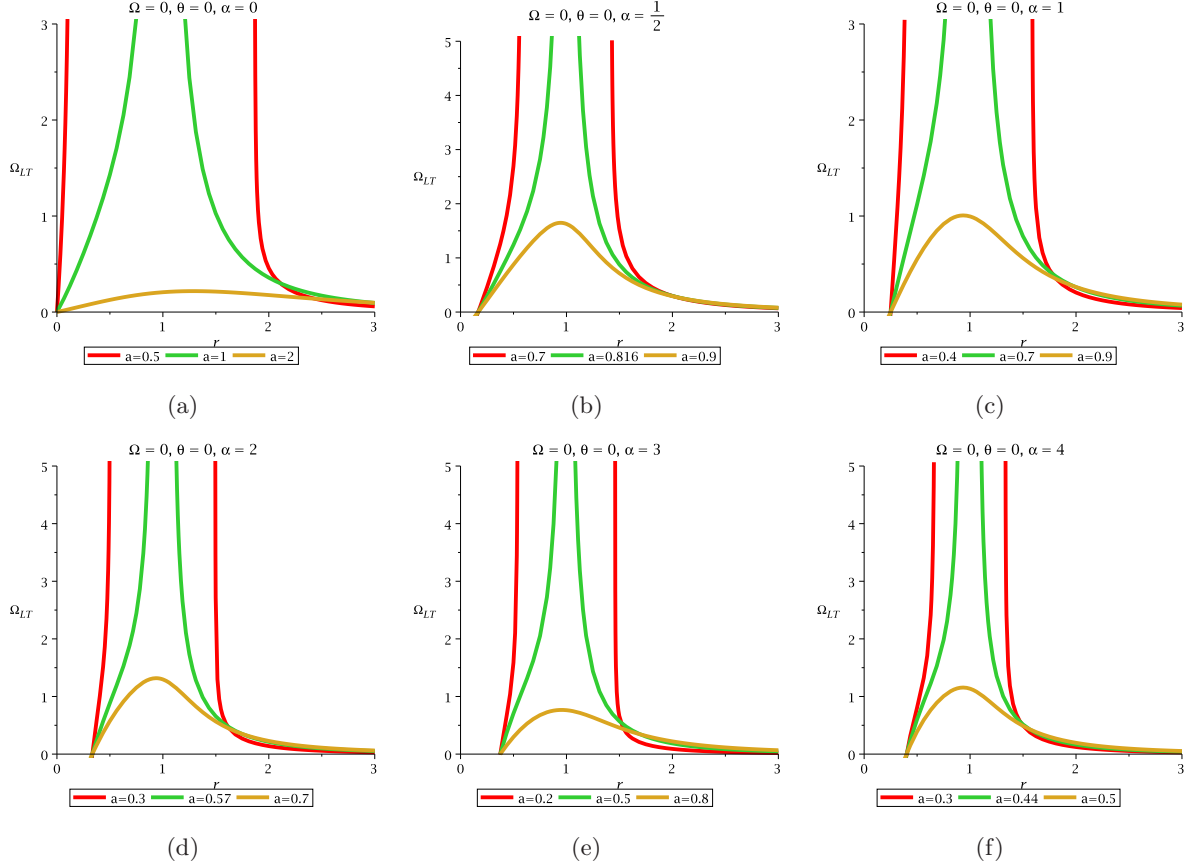


Figure 14: Examples of the variation of  $\Omega_{LT}$  versus  $r$  for  $\theta = 0$  in KMOG with variation of MOG parameter and spin parameter. Here  $\Omega = 0$ . The first figure describes the variation of  $\Omega_{LT}$  with  $r$  for non-extremal BH, extremal BH and NS without MOG parameter. The rest of the figure describes the variation of  $\Omega_{LT}$  with  $r$  for non-extremal BH, extremal BH and NS with MOG parameter. Using these plots one can easily distinguish between three compact objects.

diagram, we have plotted the LT frequency  $\Omega_{LT}$  with respect to the radial coordinate for angular coordinate value  $\theta = 0$ . We have speculated that the LT frequency is diminished due to the presence of the MOG parameter in compared to Kerr BH.

### 3.2 Behaviour of $\vec{\Omega}_{LT}$ at $\theta = \frac{\pi}{6}$

In this limit  $\theta = \frac{\pi}{6}$ , the LT frequency is computed as

$$\vec{\Omega}_{LT}|_{\theta=\frac{\pi}{6}} = \frac{\sqrt{3\Delta}\chi(r)|_{\theta=\frac{\pi}{6}}\hat{r} + \mu(r)|_{\theta=\frac{\pi}{6}}\hat{\theta}}{2\sigma(r)|_{\theta=\frac{\pi}{6}}}, \quad (114)$$

The magnitude of this vector is calculated to be

$$\Omega_{LT}|_{\theta=\frac{\pi}{6}} = \frac{\sqrt{3\Delta\chi^2(r)|_{\theta=\frac{\pi}{6}} + \mu^2(r)|_{\theta=\frac{\pi}{6}}}}{2\sigma(r)|_{\theta=\frac{\pi}{6}}} \quad (115)$$

where

$$\chi(r)|_{\theta=\frac{\pi}{6}} = a\Pi_\alpha \quad (116)$$

$$\mu(r)|_{\theta=\frac{\pi}{6}} = aG_N\mathcal{M}\left(r^2 - \frac{3}{4}a^2\right) - \frac{\alpha}{1+\alpha}G_N^2\mathcal{M}^2ar$$

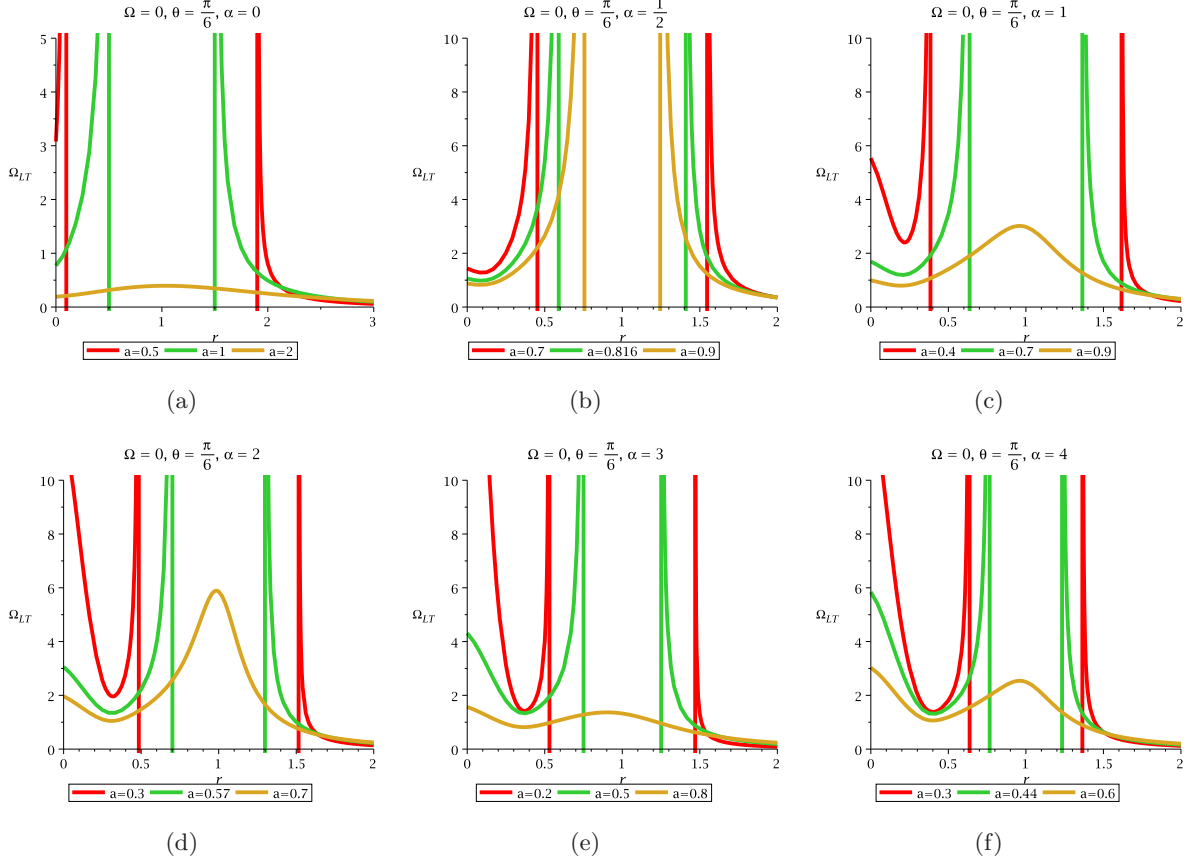


Figure 15: Examples of the variation of  $\Omega_{LT}$  versus  $r$  for  $\theta = \frac{\pi}{6}$  in KMOG with variation of MOG parameter and spin parameter. Here  $\Omega = 0$ . The first figure describes the variation of  $\Omega_{LT}$  with  $r$  for non-extremal BH, extremal BH and NS without MOG parameter. The rest of the figure describes the variation of  $\Omega_{LT}$  with  $r$  for non-extremal BH, extremal BH and NS with MOG parameter.

and

$$\sigma(r)|_{\theta=\frac{\pi}{6}} = \left(r^2 + \frac{3}{4}a^2\right)^{\frac{3}{2}} \left[\left(r^2 + \frac{3}{4}a^2\right) - \Pi_\alpha\right]$$

From the above equation one can easily see that the LT frequency is dependent on the MOG parameter and spin parameter. It could be seen from the diagram (15) by plotting the LT precession frequency with the radial coordinate.

### 3.3 Behaviour of $\vec{\Omega}_{LT}$ at $\theta = \frac{\pi}{4}$

In the limit  $\theta = \frac{\pi}{4}$ , the LT frequency is computed to be

$$\vec{\Omega}_{LT}|_{\theta=\frac{\pi}{4}} = \frac{\sqrt{\Delta}\chi(r)|_{\theta=\frac{\pi}{4}}\hat{r} + \mu(r)|_{\theta=\frac{\pi}{4}}\hat{\theta}}{\sqrt{2}\sigma(r)|_{\theta=\frac{\pi}{4}}}, \quad (117)$$

The magnitude of this vector is thus

$$\Omega_{LT}|_{\theta=\frac{\pi}{4}} = \frac{\sqrt{\Delta\chi^2(r)|_{\theta=\frac{\pi}{4}} + \mu^2(r)|_{\theta=\frac{\pi}{4}}}}{\sqrt{2}\sigma(r)|_{\theta=\frac{\pi}{4}}} \quad (118)$$

where

$$\chi(r)|_{\theta=\frac{\pi}{4}} = a\Pi_\alpha \quad (119)$$

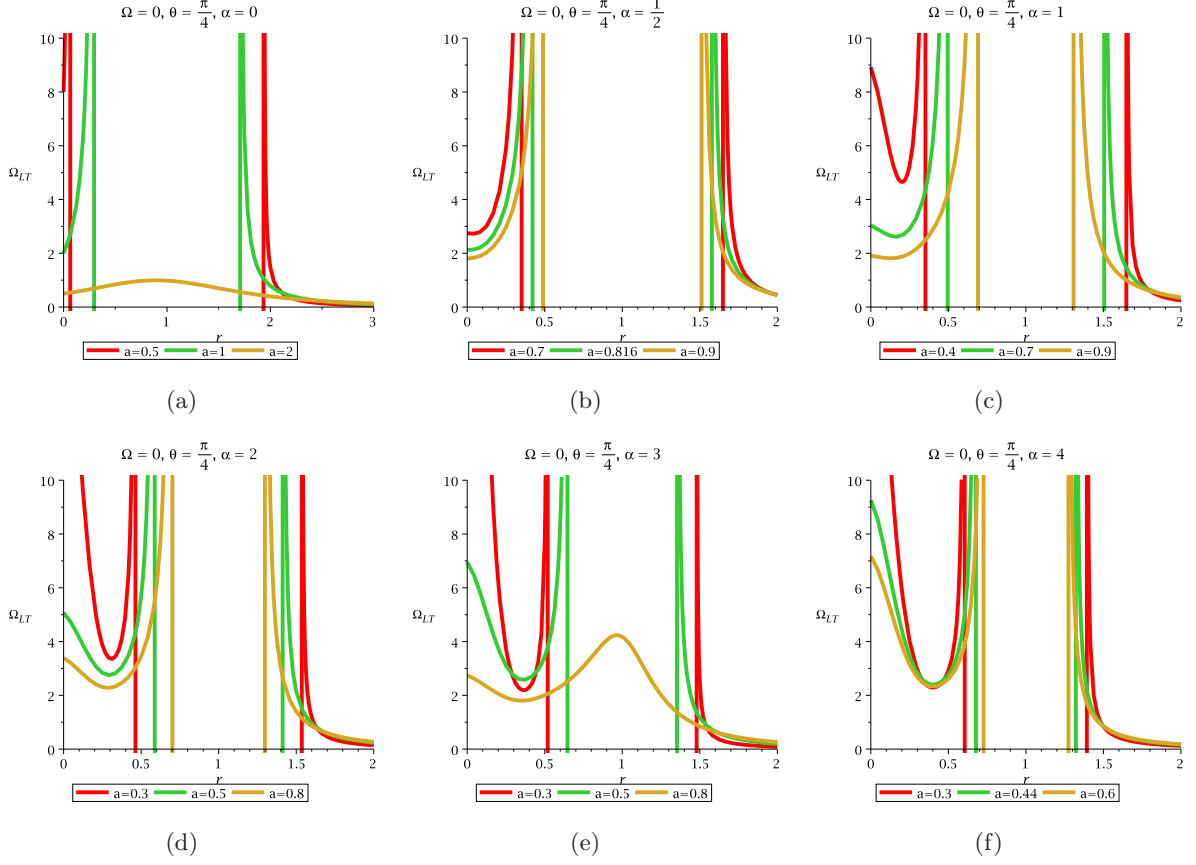


Figure 16: Examples of the variation of  $\Omega_{LT}$  versus  $r$  for  $\theta = \frac{\pi}{4}$  in KMOG with variation of MOG parameter and spin parameter. Here  $\Omega = 0$ . The first figure describes the variation of  $\Omega_{LT}$  with  $r$  for non-extremal BH, extremal BH and NS without MOG parameter. The rest of the figure describes the variation of  $\Omega_{LT}$  with  $r$  for non-extremal BH, extremal BH and NS with MOG parameter.

$$\mu(r)|_{\theta=\frac{\pi}{4}} = aG_N\mathcal{M}\left(r^2 - \frac{a^2}{2}\right) - \frac{\alpha}{1+\alpha}G_N^2\mathcal{M}^2ar$$

$$\sigma(r)|_{\theta=\frac{\pi}{4}} = \left(r^2 + \frac{a^2}{2}\right)^{\frac{3}{2}} \left[\left(r^2 + \frac{a^2}{2}\right) - \Pi_\alpha\right]$$

One could differentiate the non-extremal BH, extremal BH and NS from the diagram (16)

### 3.4 Behaviour of $\vec{\Omega}_{LT}$ at $\theta = \frac{\pi}{3}$

Similarly for  $\theta = \frac{\pi}{3}$ , the LT frequency is

$$\vec{\Omega}_{LT}|_{\theta=\frac{\pi}{3}} = \frac{\sqrt{\Delta}\chi(r)|_{\theta=\frac{\pi}{3}}\hat{r} + \sqrt{3}\mu(r)|_{\theta=\frac{\pi}{3}}\hat{\theta}}{2\sigma(r)|_{\theta=\frac{\pi}{3}}}, \quad (120)$$

The magnitude of this vector is given by

$$\Omega_{LT}|_{\theta=\frac{\pi}{3}} = \frac{\sqrt{\Delta\chi^2(r)|_{\theta=\frac{\pi}{3}} + 3\mu^2(r)|_{\theta=\frac{\pi}{3}}}}{2\sigma(r)|_{\theta=\frac{\pi}{3}}} \quad (121)$$

where

$$\chi(r)|_{\theta=\frac{\pi}{3}} = a\Pi_\alpha \quad (122)$$

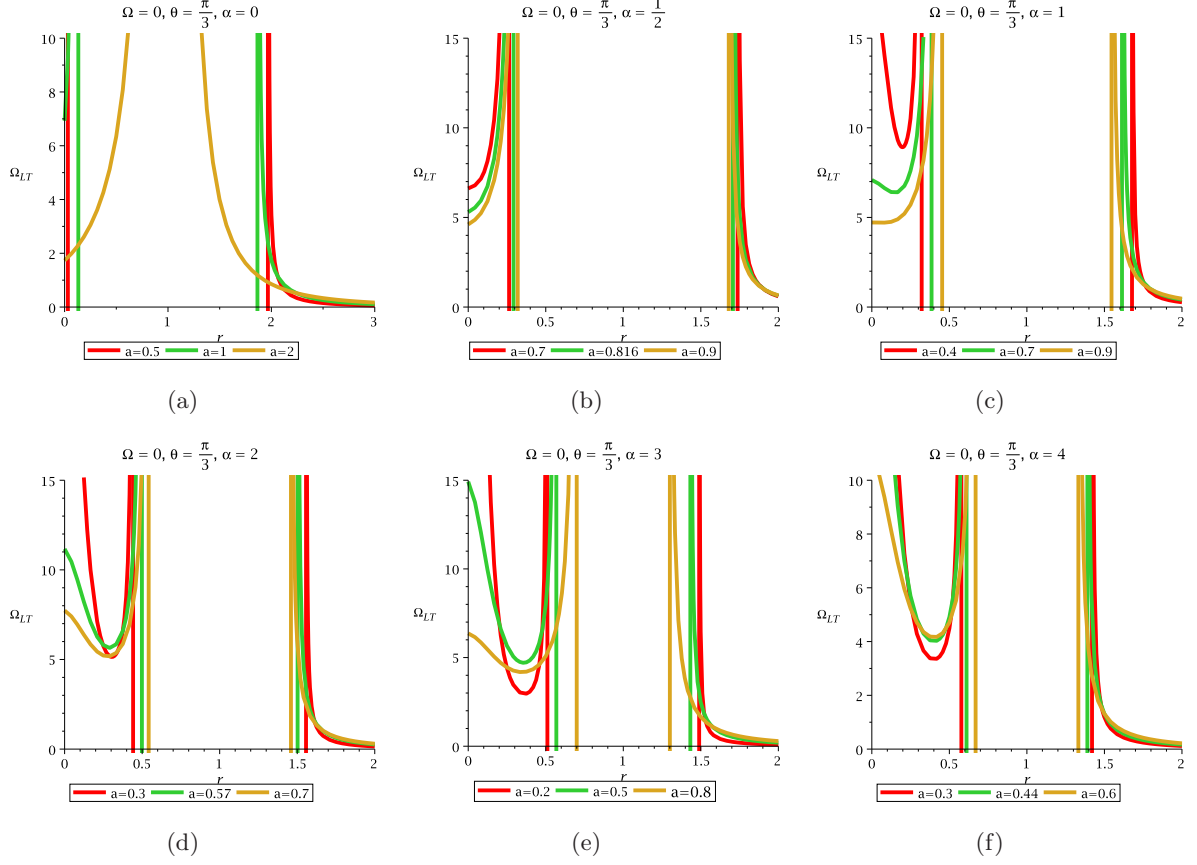


Figure 17: Examples of the variation of  $\Omega_{LT}$  versus  $r$  for  $\theta = \frac{\pi}{3}$  in KMOG with variation of MOG parameter and spin parameter. Here  $\Omega = 0$ . The first figure describes the variation of  $\Omega_{LT}$  with  $r$  for non-extremal BH, extremal BH and NS without MOG parameter. The rest of the figure describes the variation of  $\Omega_{LT}$  with  $r$  for non-extremal BH, extremal BH and NS with MOG parameter.

$$\mu(r)|_{\theta=\frac{\pi}{3}} = aG_N\mathcal{M}\left(r^2 - \frac{a^2}{4}\right) - \frac{\alpha}{1+\alpha}G_N^2\mathcal{M}^2ar$$

and

$$\sigma(r)|_{\theta=\frac{\pi}{3}} = \left(r^2 + \frac{a^2}{4}\right)^{\frac{3}{2}} \left[\left(r^2 + \frac{a^2}{4}\right) - \Pi_\alpha\right]$$

Variation of spin precession frequency with radial coordinates for various values of spin parameter could be seen from the Fig. (17).

### 3.5 Behaviour of $\vec{\Omega}_{LT}$ at $\theta = \frac{\pi}{2}$

On the equatorial plane the precession frequency vector is given by

$$\vec{\Omega}_{LT}|_{\theta=\frac{\pi}{2}} = \frac{\mu(r)|_{\theta=\frac{\pi}{2}}}{\sigma(r)|_{\theta=\frac{\pi}{2}}} \hat{\theta} \quad (123)$$

The magnitude of this vector is then

$$\Omega_{LT}|_{\theta=\frac{\pi}{2}} = \frac{\mu(r)|_{\theta=\frac{\pi}{2}}}{\sigma(r)|_{\theta=\frac{\pi}{2}}} \quad (124)$$

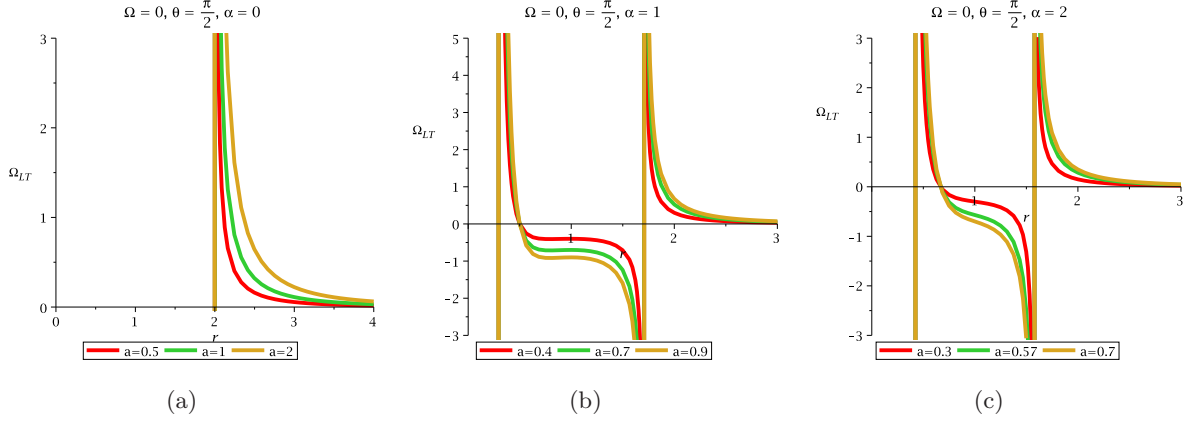


Figure 18: Examples of the variation of  $\Omega_{LT}$  versus  $r$  for  $\theta = \frac{\pi}{2}$  in KMOG with variation of MOG parameter and spin parameter. Here  $\Omega = 0$ . The first figure describes the variation of  $\Omega_{LT}$  with  $r$  for non-extremal BH, extremal BH and NS without MOG parameter. The second and third figure describes the variation of  $\Omega_{LT}$  with  $r$  for non-extremal BH, extremal BH and NS with MOG parameter.

where

$$\mu(r)|_{\theta=\frac{\pi}{2}} = ar \left( G_N \mathcal{M} r - \frac{\alpha}{1+\alpha} G_N^2 \mathcal{M}^2 \right) \quad (125)$$

$$\sigma(r)|_{\theta=\frac{\pi}{2}} = r^3 (r^2 - \Pi_\alpha) \quad (126)$$

Variation of spin precession frequency with radial coordinates for various values of spin parameter could be seen from the Fig. (18).

Using these plots, one can differentiate between non-extremal BH, extremal BH and NS in KMOG spacetime and Kerr spacetime. It could be easily say that the presence of the MOG parameter drastically changes the geometry of the BH spacetime. More appropriately, one could say that the presence of the MOG parameter enormously changes the shape of the LT frequency diagram in contrast with the zero MOG parameter LT frequency diagram. Furthermore, it is observed that in the NS case the geometric structure drastically different from BH spacetime.

### 3.6 Lense-Thirring Precession in Extremal KMOG spacetime

It is very crucial to study the LT precession in case of extremal KMOG BH in comparison to extremal Kerr BH. This is because the extremal BH has several important features. One crucial feature is that it has no Hawking temperature i.e.  $T_H = 0$ . It has also no bifurcation 2-sphere. Moreover, it has no trapped surface. Whereas its near-extremal counterpart possesses all the said features. Extremal BHs also playing a major role both in string theory and quantum gravity. They have used to count the string states in string theory while in quantum gravity they have used as a theoretical toy. In supersymmetric theory, extremal BHs satisfied the BPS (Bogomolnyi-Prasad-Sommerfield) bound and they are invariant under several super charges. They are also stable and do not radiate Hawking radiation. Their entropy was calculated in string theory [44]. The other definition of extremal BH is that it is a BH when two horizons are coincident. The extremal limit of KMOG BH is defined by  $a = \frac{G_N \mathcal{M}}{\sqrt{1+\alpha}}$  or  $J = \frac{G_N^2 \mathcal{M}^2}{\sqrt{1+\alpha}}$ . Thus one gets the extremal horizon is at  $r_{ex} = G_N \mathcal{M} = a\sqrt{1+\alpha}$ . So far we have not written the exact expression of LT precession frequency vector for extremal KMOG BH now we should write this expression as

$$\vec{\Omega}_{LT} = \frac{G_N \mathcal{M}}{\sqrt{1+\alpha}} \times$$

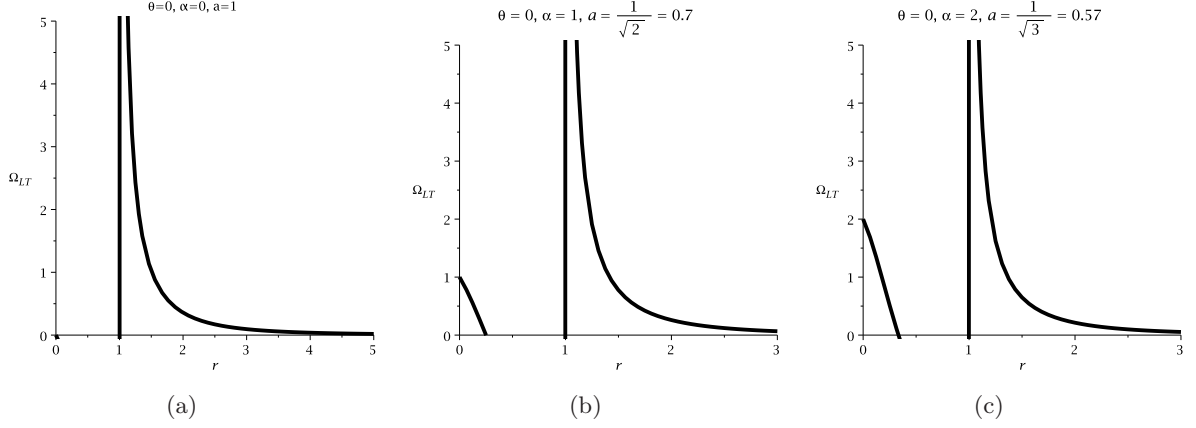


Figure 19: The first figure describes the variation of  $\Omega_{LT}$  with  $r$  for extremal BH in KMOG without MOG parameter. The second and third figure describes the variation of  $\Omega_{LT}$  with  $r$  for extremal BH with MOG parameter. Here we set  $\theta = 0$ .

$$\frac{\left[ \Pi_\alpha (r - G_N \mathcal{M}) \cos \theta \hat{r} + G_N \mathcal{M} \left( r^2 - \frac{\alpha}{1+\alpha} G_N \mathcal{M} r - \frac{G_N^2 \mathcal{M}^2}{1+\alpha} \cos^2 \theta \right) \sin \theta \hat{\theta} \right]}{\left( r^2 + \frac{G_N^2 \mathcal{M}^2}{1+\alpha} \cos^2 \theta \right)^{\frac{3}{2}} \left( r^2 - \Pi_\alpha + \frac{G_N^2 \mathcal{M}^2}{1+\alpha} \cos^2 \theta \right)} \quad (127)$$

Taking magnitude of this vector one obtains the LT frequency for extremal KMOG BH as

$$\Omega_{LT}(r, \theta, \alpha) = \frac{G_N \mathcal{M}}{\sqrt{1+\alpha}} \times \frac{\left[ \Pi_\alpha^2 (r - G_N \mathcal{M})^2 \cos^2 \theta + G_N^2 \mathcal{M}^2 \left( r^2 - \frac{\alpha}{1+\alpha} G_N \mathcal{M} r - \frac{G_N^2 \mathcal{M}^2}{1+\alpha} \cos^2 \theta \right)^2 \sin^2 \theta \right]^{\frac{1}{2}}}{\left( r^2 + \frac{G_N^2 \mathcal{M}^2}{1+\alpha} \cos^2 \theta \right)^{\frac{3}{2}} \left( r^2 - \Pi_\alpha + \frac{G_N^2 \mathcal{M}^2}{1+\alpha} \cos^2 \theta \right)} \quad (128)$$

Now we will compute the LT frequency of extremal KMOG BH for various angles starting from polar region to equatorial plane and the variation of the said frequency could be observed from the plot.

Case I:

First we take the value of  $\theta = 0$ , then one gets the LT frequency as

$$\Omega_{LT} = \frac{G_N \mathcal{M}}{\sqrt{1+\alpha}} \frac{\Pi_\alpha}{\left( r^2 + \frac{G_N^2 \mathcal{M}^2}{1+\alpha} \right)^{\frac{3}{2}} (r - G_N \mathcal{M})} = f(r, \mathcal{M}, \alpha) \quad (129)$$

It follows that the frequency is a function of  $f(r, \mathcal{M}, \alpha)$  while for Kerr BH it is a function of  $f(r, \mathcal{M})$  only. It also should be noted that at the extremal horizon the LT frequency diverges both for extremal KMOG and extremal Kerr BH. Variation of Lense-Thirring frequency of extremal KMOG BH could be observed from Fig. (19) for different spin values.

Case II:

For  $\theta = \frac{\pi}{6}$ , the LT frequency is derived to be

$$\Omega_{LT}(r, \frac{\pi}{6}) = \frac{G_N \mathcal{M}}{2\sqrt{1+\alpha}} \times \frac{\left[ 3\Pi_\alpha^2 (r - G_N \mathcal{M})^2 + G_N^2 \mathcal{M}^2 \left( r^2 - \frac{\alpha}{1+\alpha} G_N \mathcal{M} r - \frac{3G_N^2 \mathcal{M}^2}{4(1+\alpha)} \right)^2 \right]^{\frac{1}{2}}}{\left[ r^2 + \frac{3G_N^2 \mathcal{M}^2}{4(1+\alpha)} \right]^{\frac{3}{2}} \left[ r^2 - \Pi_\alpha + \frac{3G_N^2 \mathcal{M}^2}{4(1+\alpha)} \right]} \quad (130)$$



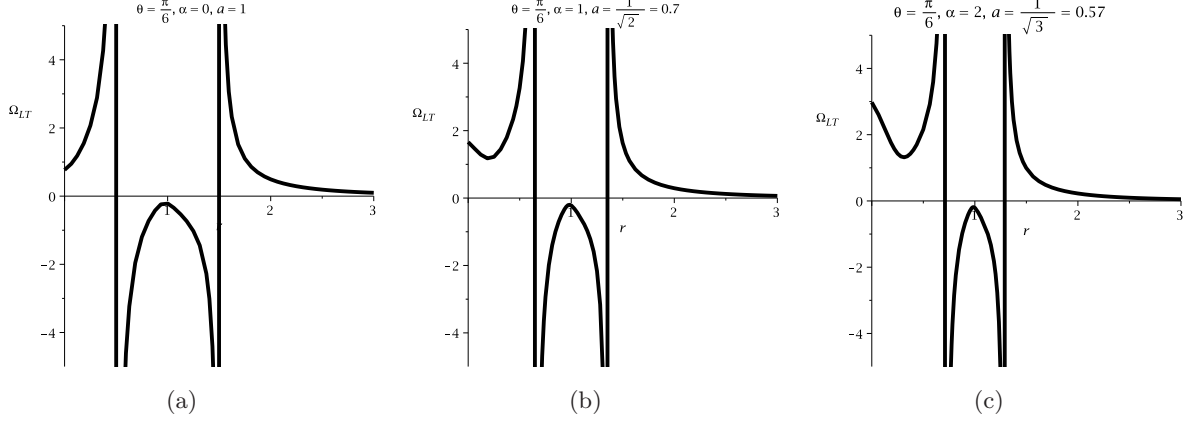


Figure 20: The first figure describes the variation of  $\Omega_{LT}$  with  $r$  for extremal BH in KMOG without MOG parameter. The second and third figure describes the variation of  $\Omega_{LT}$  with  $r$  for extremal BH in KMOG with MOG parameter. Here we set  $\theta = \frac{\pi}{6}$ .

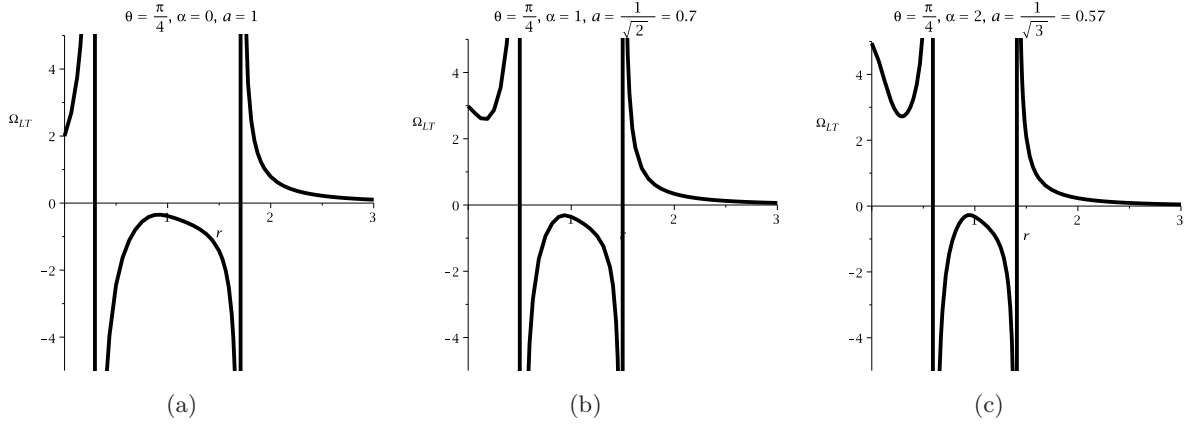


Figure 21: The first figure describes the variation of  $\Omega_{LT}$  with  $r$  for extremal BH in KMOG without MOG parameter. The second and third figure describes the variation of  $\Omega_{LT}$  with  $r$  for extremal BH in KMOG with MOG parameter. Here we set  $\theta = \frac{\pi}{4}$ .

Case III:

For  $\theta = \frac{\pi}{4}$ , the LT frequency is computed to be

$$\Omega_{LT}(r, \frac{\pi}{4}) = \frac{G_N \mathcal{M}}{\sqrt{2(1+\alpha)}} \times \frac{\left[ \Pi_\alpha^2 (r - G_N \mathcal{M})^2 + G_N^2 \mathcal{M}^2 \left( r^2 - \frac{\alpha}{1+\alpha} G_N \mathcal{M} r - \frac{G_N^2 \mathcal{M}^2}{2(1+\alpha)} \right)^2 \right]^{\frac{1}{2}}}{\left[ r^2 + \frac{G_N^2 \mathcal{M}^2}{2(1+\alpha)} \right]^{\frac{3}{2}} \left[ r^2 - \Pi_\alpha + \frac{G_N^2 \mathcal{M}^2}{2(1+\alpha)} \right]} \quad (131)$$

Case IV:

For  $\theta = \frac{\pi}{3}$ , the LT frequency is derived to be

$$\Omega_{LT}(r, \frac{\pi}{3}) = \frac{G_N \mathcal{M}}{2\sqrt{1+\alpha}} \times$$

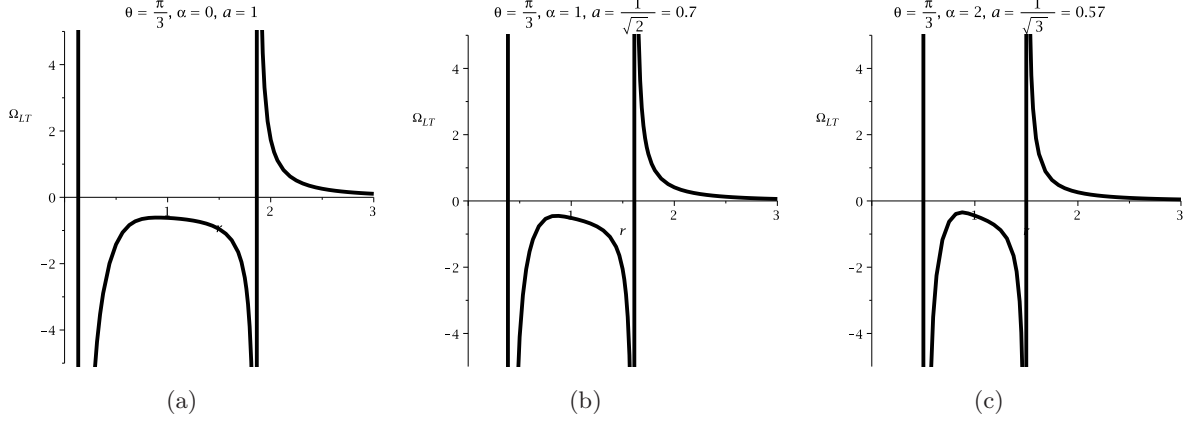


Figure 22: The first figure describes the variation of  $\Omega_{LT}$  with  $r$  for extremal BH in KMOG without MOG parameter. The second and third figure describes the variation of  $\Omega_{LT}$  with  $r$  for extremal BH in KMOG with MOG parameter. Here we set  $\theta = \frac{\pi}{3}$ .

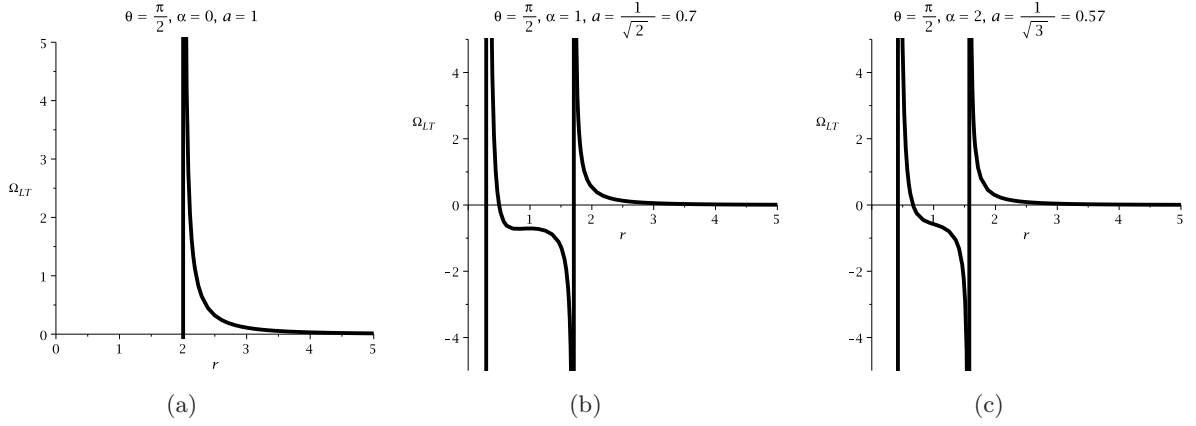


Figure 23: The first figure describes the variation of  $\Omega_{LT}$  with  $r$  for extremal BH in KMOG without MOG parameter. The second and third figure describes the variation of  $\Omega_{LT}$  with  $r$  for extremal BH in KMOG with MOG parameter. Here we set  $\theta = \frac{\pi}{2}$ .

$$\frac{\left[ \Pi_{\alpha}^2 (r - G_N \mathcal{M})^2 + 3G_N^2 \mathcal{M}^2 \left( r^2 - \frac{\alpha}{1+\alpha} G_N \mathcal{M} r - \frac{G_N^2 \mathcal{M}^2}{4(1+\alpha)} \right)^2 \right]^{\frac{1}{2}}}{\left[ r^2 + \frac{G_N^2 \mathcal{M}^2}{4(1+\alpha)} \right]^{\frac{3}{2}} \left[ r^2 - \Pi_{\alpha} + \frac{G_N^2 \mathcal{M}^2}{4(1+\alpha)} \right]} \quad (132)$$

Case V:

Finally, for  $\theta = \frac{\pi}{2}$ , the LT frequency is

$$\Omega_{LT} = \frac{G_N^2 \mathcal{M}^2 \left( r - \frac{\alpha}{1+\alpha} G_N \mathcal{M} \right)}{\sqrt{1+\alpha} r^2 (r^2 - \Pi_{\alpha})} \quad (133)$$

It should be noted that in each cases the LT frequency reduces to Kerr BH for  $\alpha = 0$ . The variation of these frequencies could be observed from following Fig. (23).

## 4 Accretion Disk properties in KMOG spacetime

To differentiate non-extremal BH spacetime, extremal BH spacetime and NS, it is essential to study accretion disk physics around a stationary, axisymmetric spacetime. To distinguish three geometries of the compact object, also it is essential to study three fundamental frequencies of accretion disk. This could be possible only by studying the geodesic motion of test particle around the compact objects. Again to study the physics of accretion disk, one should compute the stable circular orbit of the said compact object. The main stable orbit is inner-most stable circular orbit (ISCO) or last stable circular orbit (LSCO). This ISCO can help us to distinguish three geometries. In Kerr geometry, the ISCO radii depends on spin parameter ( $a$ ) while in KMOG geometry, it depends on both spin parameter ( $a_\alpha$ ) and MOG parameter ( $\alpha$ ). We previously noticed that in KMOG geometry, the spin parameter decreases as MOG value increases (See Fig. (2)).

Three fundamental frequencies which are very important for accretion disk physics of KMOG BH, namely the Keplerian frequency ( $\Omega_\phi$ ), the radial epicyclic frequency ( $\Omega_r$ ) and the vertical epicyclic frequency ( $\Omega_\theta$ ). They can easily be derived using the formulae (145,146,147) given in Appendix: [See also [35]]<sup>5</sup>

$$\Omega_\phi = \pm \frac{\sqrt{\Pi_\alpha - G_N \mathcal{M} r}}{r^2 \pm a \sqrt{\Pi_\alpha - G_N \mathcal{M} r}} \quad (134)$$

$$\Omega_r = \frac{\sqrt{G_N \mathcal{M} r \Delta - 4(\Pi_\alpha - G_N \mathcal{M} r)(\sqrt{\Pi_\alpha - G_N \mathcal{M} r} \mp a)^2}}{r(r^2 \pm a \sqrt{\Pi_\alpha - G_N \mathcal{M} r})} \quad (135)$$

$$\Omega_\theta = \frac{\sqrt{r^2(\Pi_\alpha - G_N \mathcal{M} r) \mp 2a\Pi_\alpha \sqrt{\Pi_\alpha - G_N \mathcal{M} r} + a^2(2\Pi_\alpha - G_N \mathcal{M} r)}}{r(r^2 \pm a \sqrt{\Pi_\alpha - G_N \mathcal{M} r})} \quad (136)$$

$$(137)$$

It is important to note that the upper sign for corotating (direct) orbit and lower sign for counter-rotating (retrograde) orbit. When MOG value vanishes, one obtains the epicyclic frequencies of Kerr BH.

The variation of these frequencies for three compact objects namely non-extremal BH, extremal BH and NS could be seen from the following diagram [Fig. (24), Fig. (25), Fig. (26)]. From first figure when  $\alpha = 0$  means that for Kerr BH, it is observed that the Keplerian frequency decreases with increasing the radial value starting from maximum value for non-extremal BH ( $a = 0.5$ ). As spin value increases the value of Keplerian frequency decreases. While in second figure where the MOG parameter is present then the picture is quite different from the former. Here the Keplerian frequency has gone through a peak for different spin values. The other two important frequency namely, the periastron precession frequency ( $\Omega_{per}$ ) and nodal precession frequency ( $\Omega_{nod}$ ) could be defined as

$$\Omega_{per} = \Omega_\phi - \Omega_r \quad (138)$$

$$\Omega_{nod} = \Omega_\phi - \Omega_\theta \quad (139)$$

All these frequencies above that we have defined are related to the precession of the orbit and orbital plane. Periastron frequency occurs due to the precession of the orbit while nodal precession frequency occurs due to the precession of orbital plane. Sometimes the nodal precession frequency is called as orbital planer precession frequency or Lense-Thirring precession frequency [2]. The radial variation of these two frequencies could be observed from Fig. (27) and Fig. (28).

The fact that  $\Omega_r^2 \geq 0$  and  $\Omega_\theta^2 \geq 0$  determined the stability of circular orbits. From the first condition one can compute radii of ISCO. It is well known that ISCO of Kerr BH is located at [47]

$$\frac{r_{ISCO}}{\mathcal{M}} = 3 + z_2 \mp \sqrt{(3 - z_1)(3 + z_1 + 2z_2)} \quad (140)$$

---

<sup>5</sup>Note that in Ref. [35] the term  $G_N$  is missing, here we have included it in each frequencies formulae

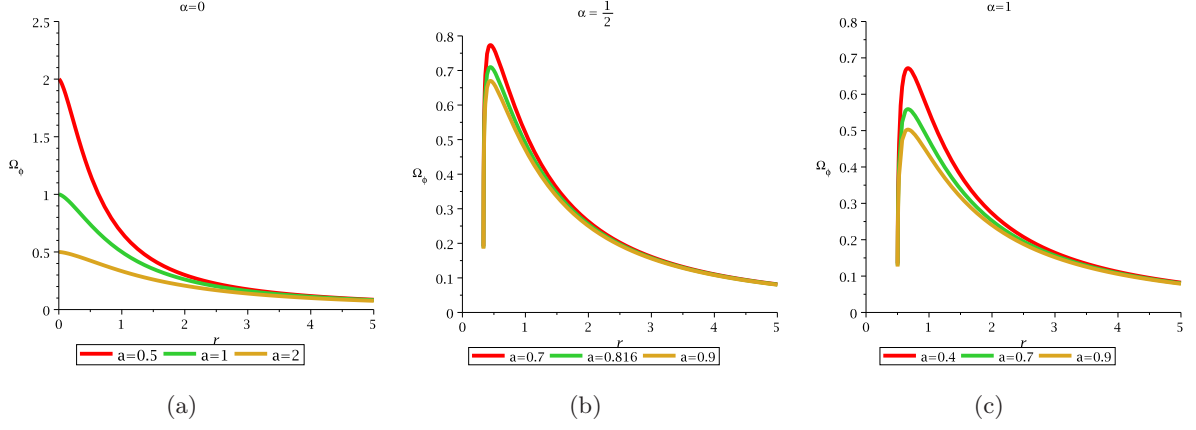


Figure 24: The figure depicts the variation of  $\Omega_\phi$  with  $r$  for different MOG parameter and spin parameter. Each figure demonstrates the difference between non-extremal BH, extremal BH and NS. Without MOG there is no peak while with MOG there exists a peak value in Keplerian frequency.

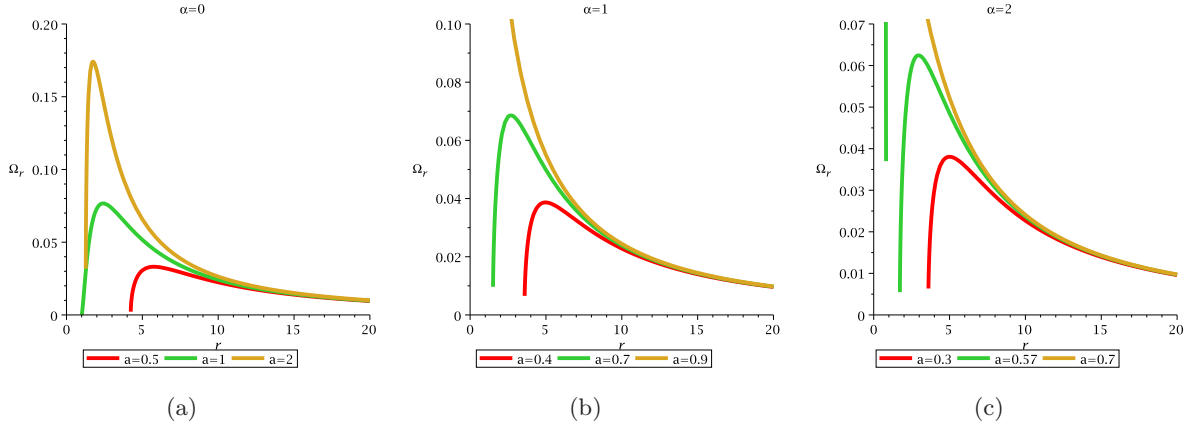


Figure 25: The figure depicts the variation of  $\Omega_r$  with  $r$  for different MOG parameter and spin parameter. Each figure shows the difference between three compact objects namely, non-extremal BH, extremal BH and NS.

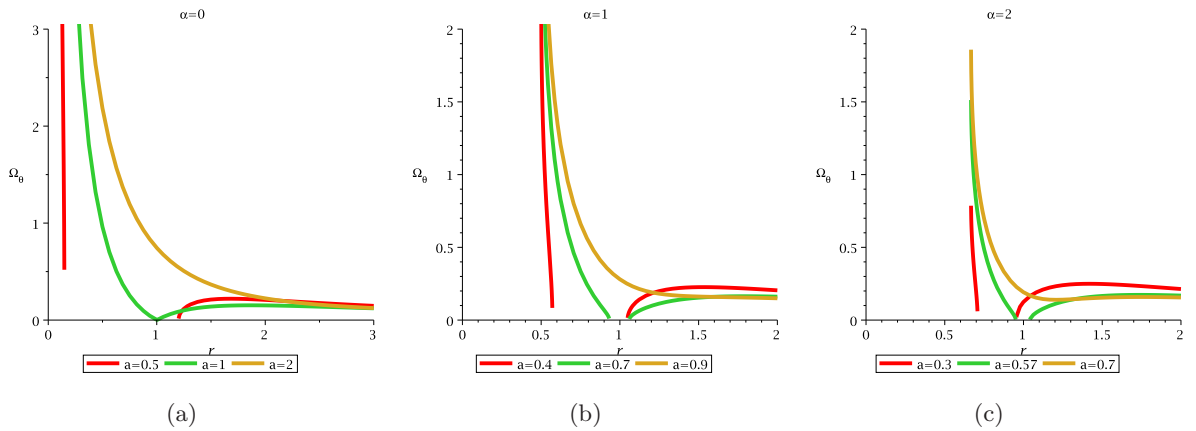


Figure 26: The figure depicts the variation of  $\Omega_\theta$  with  $r$  for different MOG parameter and spin parameter. Each figure characterizes the difference between non-extremal BH, extremal BH and NS.

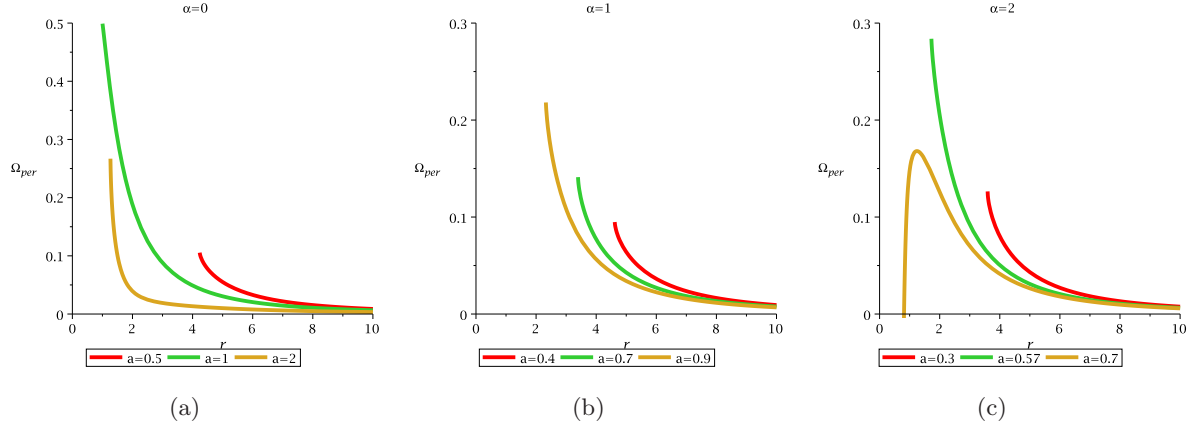


Figure 27: The figure depicts the variation of  $\Omega_{per}$  with  $r$  for different MOG parameter and spin parameter. Each figure shows the difference between non-extremal BH, extremal BH and NS.

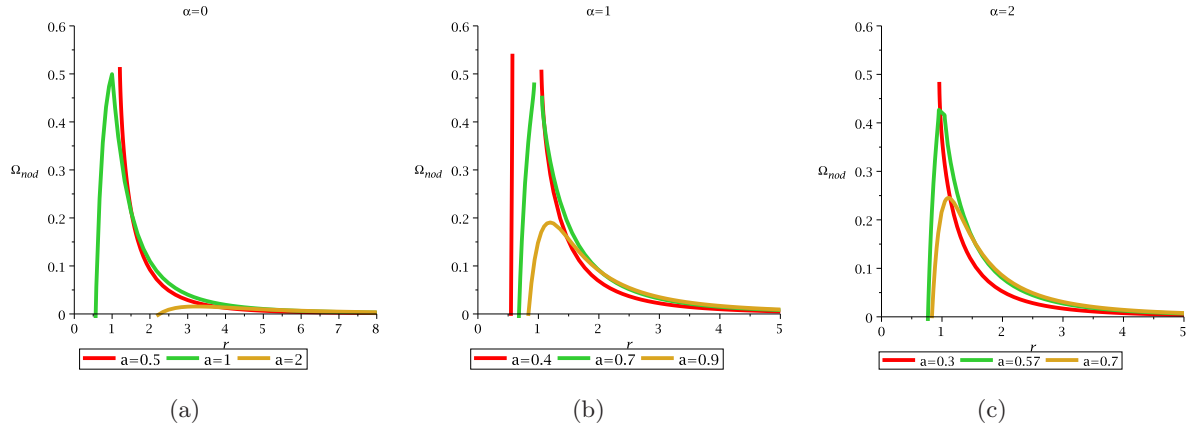


Figure 28: The figure depicts the variation of  $\Omega_{nod}$  with  $r$  for different MOG parameter and spin parameter. Each figure classifies the difference between non-extremal BH, extremal BH and NS.

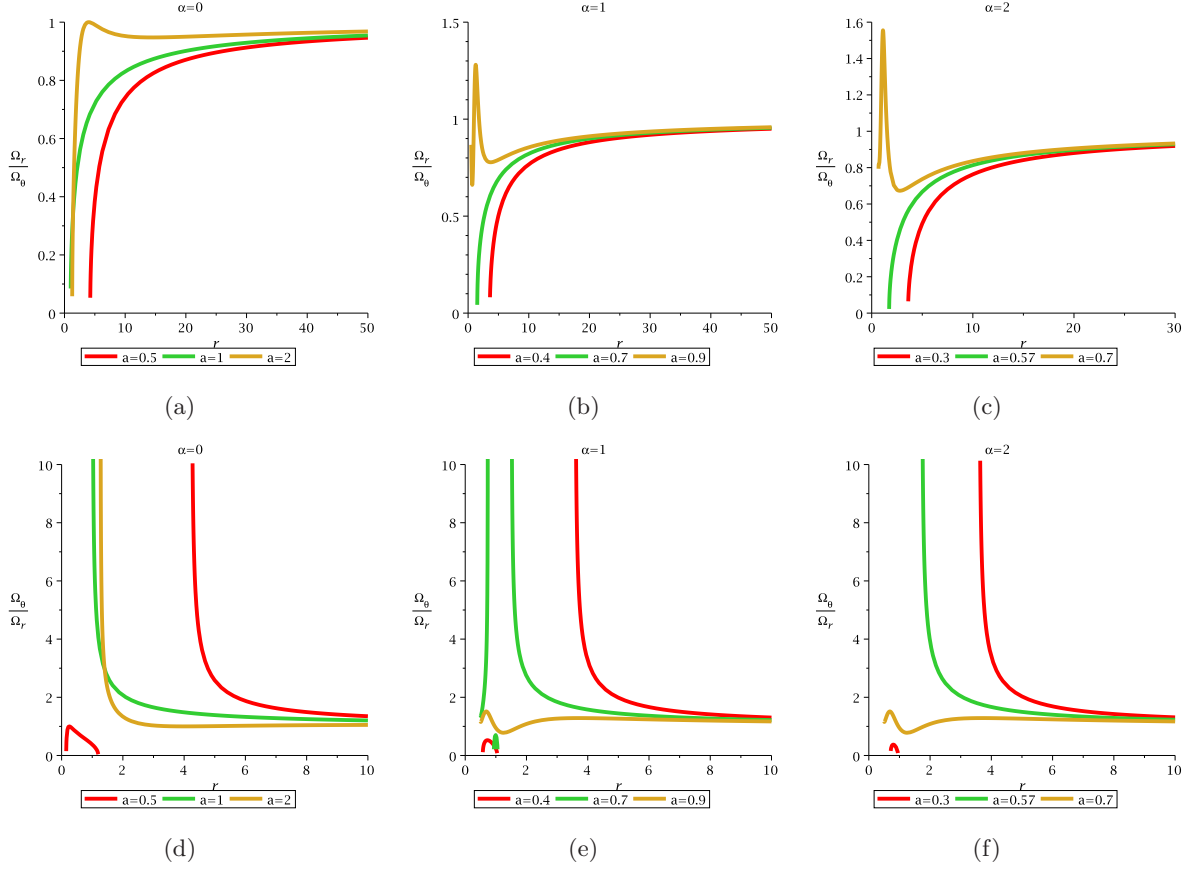


Figure 29: The figure depicts the variation of  $\frac{\Omega_r}{\Omega_\theta}$  and  $\frac{\Omega_\theta}{\Omega_r}$  with  $r$  for different MOG parameter and spin parameter. Each figure depicts the difference between non-extremal BH, extremal BH and NS.

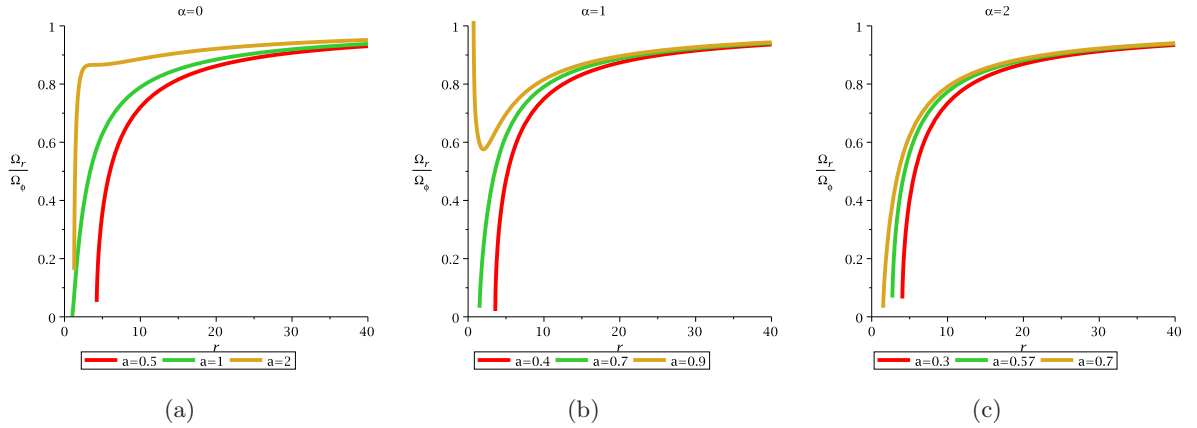


Figure 30: The figure depicts the variation of  $\frac{\Omega_r}{\Omega_\phi}$  with  $r$  for different MOG parameter and spin parameter. Each figure depicts the difference between non-extremal BH, extremal BH and NS.

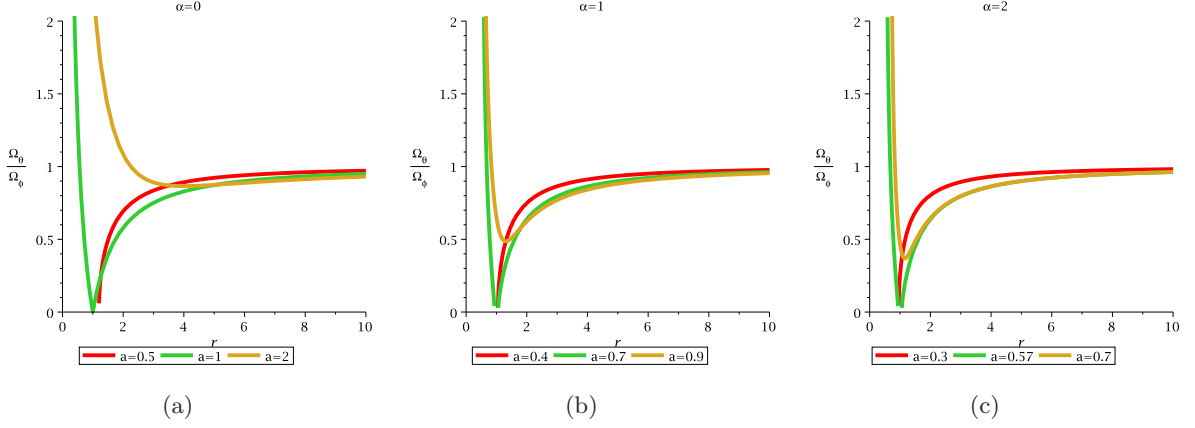


Figure 31: The figure depicts the variation of  $\frac{\Omega_r}{\Omega_\phi}$  with  $r$  for different MOG parameter and spin parameter. Each figure depicts the difference between non-extremal BH, extremal BH and NS.

where

$$z_1 = 1 + \left(1 - \frac{a^2}{\mathcal{M}^2}\right)^{1/3} \left[\left(1 - \frac{a}{\mathcal{M}}\right)^{1/3} + \left(1 + \frac{a}{\mathcal{M}}\right)^{1/3}\right] \quad (141)$$

$$z_2 = \sqrt{3 \frac{a^2}{\mathcal{M}^2} + z_1^2} \quad (142)$$

Here, upper sign indicates direct orbit and lower sign indicates retrograde orbit. For extremal Kerr BH, the ISCO is situated at  $r_{ISCO} = \mathcal{M}$  for direct orbit while  $r_{ISCO} = 9\mathcal{M}$  for retrograde orbit [47]. The non-negativeness of  $\Omega_\theta$  implies that the geodesic motion is stable under small oscillations in the vertical direction. While in KMOG BH, the ISCO radii can be calculated via the equation  $\Omega_r^2 = 0$ :

$$G_N \mathcal{M} r \Delta - 4(\Pi_\alpha - G_N \mathcal{M} r) \left(\sqrt{\Pi_\alpha - G_N \mathcal{M} r} \mp a\right)^2 = 0$$

In spherically symmetric spacetime where the value of spin parameter  $a = 0$  means that  $\Omega_\phi = \Omega_\theta$ , which implies that the Lense-Thirring precession is absent while in axisymmetric spacetime  $\Omega_\phi \neq \Omega_\theta$ . This will be vanish for a particular value of  $r = r_0$  i.e.

$$\Omega_{nod}|_{r=r_0} = 0$$

which implies that

$$4\Pi_\alpha^2 \frac{(\Pi_\alpha - G_N \mathcal{M} r)}{(2\Pi_\alpha - G_N \mathcal{M} r)^2} \Big|_{r=r_0} = a^2$$

when MOG parameter vanishes it reduces to

$$\frac{16}{9} \frac{r_0}{\mathcal{M}} = a^2$$

We can differentiate three compact objects via ratio of two epicyclic frequencies (plot for direct orbit only) which is defined to be as follows

$$\frac{\Omega_r}{\Omega_\theta} = \frac{\sqrt{G_N \mathcal{M} r \Delta - 4(\Pi_\alpha - G_N \mathcal{M} r) (\sqrt{\Pi_\alpha - G_N \mathcal{M} r} \mp a)^2}}{\sqrt{r^2 (\Pi_\alpha - G_N \mathcal{M} r) \mp 2a\Pi_\alpha \sqrt{\Pi_\alpha - G_N \mathcal{M} r} + a^2 (2\Pi_\alpha - G_N \mathcal{M} r)}}$$

$$\frac{\Omega_r}{\Omega_\phi} = \pm \frac{\sqrt{G_N \mathcal{M} r \Delta - 4(\Pi_\alpha - G_N \mathcal{M} r) (\sqrt{\Pi_\alpha - G_N \mathcal{M} r} \mp a)^2}}{r \sqrt{\Pi_\alpha - G_N \mathcal{M} r}}$$

$$\frac{\Omega_\theta}{\Omega_\phi} = \pm \frac{\sqrt{r^2 (\Pi_\alpha - G_N \mathcal{M}r) \mp 2a\Pi_\alpha \sqrt{\Pi_\alpha - G_N \mathcal{M}r} + a^2 (2\Pi_\alpha - G_N \mathcal{M}r)}}{r\sqrt{\Pi_\alpha - G_N \mathcal{M}r}}$$

The variation of these ratio may be seen from the following diagram [(29), (30), (31)].

## 5 Discussion

We performed a detailed analysis of the inertial frame-dragging effect of stationary, axisymmetric KMOG BH. Specifically, we computed the generalized spin precession of a test gyroscope due to frame-dragging effect when it is placed in the domain of the BH as well as NS. By computing this frequency, we distinguished the behaviour of three astrophysical compact objects namely non-extremal BH, extremal BH and NS. We showed in principle a clear distinction between these three compact objects visually. We also compared this result with the Kerr BH. We studied different features in MOG by using spin precession versus radial profile. In each spin precession vs. radial diagram, we observed distinguished features of three compact objects for various spin limits.

Perhaps the most promising result we obtained is that the presence of the MOG parameter deformed the geometric construction of different essential parameters like event horizon ( $r_+$ ), Cauchy horizon ( $r_-$ ), outer ergosphere ( $r_e^+$ ), inner ergosphere ( $r_e^-$ ), generalized spin frequency ( $\Omega_p$ ), LT frequency ( $\Omega_{LT}$ ) etc. in contrast to zero MOG parameter.

We also investigated the generalized spin precession frequency for various angular limits:  $\theta = 0$ ,  $\theta = \frac{\pi}{6}$ ,  $\theta = \frac{\pi}{4}$ ,  $\theta = \frac{\pi}{3}$  and finally  $\theta = \frac{\pi}{2}$ . Moreover, we studied the generalized spin frequency for ring singularity. Then we studied the frame-dragging effect with vanishing angular velocity. This means that we derived the LT frequency only by omitting the other frequencies. We showed that the LT frequency is affected by the MOG parameter. It is clearly observed from LT frequency vs. radial diagram. For vanishing  $\Omega = 0$ , we also studied the LT frequency for angular values:  $\theta = 0$ ,  $\theta = \frac{\pi}{6}$ ,  $\theta = \frac{\pi}{4}$ ,  $\theta = \frac{\pi}{3}$  and  $\theta = \frac{\pi}{2}$ . Each diagram clearly showed the distinction between three compact objects namely, non-extremal BH, extremal BH and NS.

Moreover, we studied the LT frequency particularly for extremal KMOG BH in compared with extremal Kerr BH. In this case we also examined the LT frequency for various angular values. From each diagram of  $\Omega_{LT}$  vs.  $r$ , we observed a diverging value of LT frequency at  $r = G_N M$ . It has been also observed that the presence of MOG parameter significantly changes the geometry of the BH spacetime in contrast to zero MOG parameter.

Finally, we studied the accretion disk properties by computing three fundamental epicyclic frequencies, namely the Keplerian frequency, radial epicyclic frequency and vertical epicyclic frequency. We also studied periastron frequency and nodal frequency. Using these properties of epicyclic frequencies, we differentiated three compact objects. From different frequency diagram, it should be clearly observed that three geometries are distinct. Furthermore, we calculated the ratio  $\frac{\Omega_r}{\Omega_\phi}$ ,  $\frac{\Omega_r}{\Omega_\theta}$  and  $\frac{\Omega_\theta}{\Omega_\phi}$ . Using these features, we differentiated three compact objects.

In summary, to test the strong gravity in MOG and to distinguish three compact objects namely the non-extremal BH, extremal BH and NS we have computed different essential parameters i. e.  $\Omega_p$ ,  $\Omega_{LT}$ ,  $\Omega_r$ ,  $\Omega_\theta$ ,  $\Omega_\phi$ ,  $\Omega_{per}$ ,  $\Omega_{nod}$ ,  $\frac{\Omega_r}{\Omega_\phi}$ ,  $\frac{\Omega_r}{\Omega_\theta}$  and  $\frac{\Omega_\theta}{\Omega_\phi}$ . By using the features of these parameters, one can distinguish between BH (non-extremal & extremal) and NS.

## Acknowledgements

I would like to thank Dr. Chandrachur Chakraborty of KIAA, China for helpful suggestions.



## A Epicyclic frequencies in a general axisymmetric and stationary spacetime

We consider a general stationary and axisymmetric spacetime as

$$ds^2 = g_{tt} dt^2 + g_{rr} dr^2 + g_{\theta\theta} d\theta^2 + g_{\phi\phi} d\phi^2 + 2g_{t\phi} d\phi dt, \quad (143)$$

where  $g_{\mu\nu} = g_{\mu\nu}(r, \theta)$ . For this spacetime the proper angular momentum ( $l$ ) of a test particle can be defined as

$$l = -\frac{g_{t\phi} + \Omega_\phi g_{\phi\phi}}{g_{tt} + \Omega_\phi g_{t\phi}}, \quad (144)$$

where,  $\Omega_\phi$  is the orbital frequency of a test particle. Now the  $\Omega_\phi$  can be defined as

$$\Omega_\phi = \frac{\dot{\phi}}{\dot{t}} = \frac{(\frac{d\phi}{d\tau})}{(\frac{dt}{d\tau})} = \frac{d\phi}{dt} = \frac{-\partial_r g_{t\phi} \pm \sqrt{(\partial_r g_{t\phi})^2 - (\partial_r g_{tt})(\partial_r g_{\phi\phi})}}{\partial_r g_{\phi\phi}} \quad (145)$$

The upper sign is for corotating orbit and the lower sign is for counterrotating orbit. The general expressions for computing the radial ( $\Omega_r$ ) and vertical ( $\Omega_\theta$ ) epicyclic frequencies are [54, 55]

$$\begin{aligned} \Omega_r^2 &= \frac{(g_{tt} + \Omega_\phi g_{t\phi})^2}{2 g_{rr}} \partial_r^2 U \\ &= \frac{(g_{tt} + \Omega_\phi g_{t\phi})^2}{2 g_{rr}} \left[ \partial_r^2 \left( \frac{g_{\phi\phi}}{Y} \right) + 2l \partial_r^2 \left( \frac{g_{t\phi}}{Y} \right) + l^2 \partial_r^2 \left( \frac{g_{tt}}{Y} \right) \right]_{r=const., \theta=\frac{\pi}{2}} \end{aligned} \quad (146)$$

and

$$\begin{aligned} \Omega_\theta^2 &= \frac{(g_{tt} + \Omega_\phi g_{t\phi})^2}{2 g_{\theta\theta}} \partial_\theta^2 U \\ &= \frac{(g_{tt} + \Omega_\phi g_{t\phi})^2}{2 g_{\theta\theta}} \left[ \partial_\theta^2 \left( \frac{g_{\phi\phi}}{Y} \right) + 2l \partial_\theta^2 \left( \frac{g_{t\phi}}{Y} \right) + l^2 \partial_\theta^2 \left( \frac{g_{tt}}{Y} \right) \right]_{r=const., \theta=\frac{\pi}{2}} \end{aligned} \quad (147)$$

respectively and  $Y$  can be defined as

$$Y = g_{tt} g_{\phi\phi} - g_{t\phi}^2. \quad (148)$$

## References

- [1] W. de Sitter, “On the bearing of the Principle of Relativity on Gravitational Astronomy”, *Mon. Not. Roy. Astron. Soc.* , **77** 155 (1916).
- [2] J. Lense and H. Thirring, “On the effect of rotating distant masses in Einstein’s theory of gravitation”, *Physikalische Zeitschrift*, **19** 156-163 (1918).
- [3] L. I. Schiff, “Possible New Experimental Test of General Relativity Theory”, *Phys. Rev. Lett* , **4** 215 (1960).
- [4] C. W. F. Everitt et al., “Gravity probe B: final results of a space experiment to test general relativity”, *Phys. Rev. Lett* , **106** 221101 (2011).
- [5] GP-B website: <http://einstein.stanford.edu>.
- [6] “The Rossi X-ray Timing Explorer Mission (1995-2012)”, <https://heasarc.gsfc.nasa.gov/docs/xte>.

- [7] Event Horizon Telescope, <https://eventhorizontelescope.org>.
- [8] R. Kannan and P. Saha, “Frame dragging and the kinematics of galactic-center stars”, *The Astrophys. J.*, **690** 1553 (2009).
- [9] F. de Felice, S. U. Tommaset, “Schwarzschild spacetime: measurements in orbiting space-stations”, *Class. Quant. Grav.*, **10** 353 (1993).
- [10] I. Ciufolini & J. A. Wheeler, “Gravitation and Inertia”, *Princeton Univ. Press, Princeton, New Jersey*, (1995).
- [11] C. M. Will, “Theory and Experiment in Gravitational Physics., 2nd edn.”, *Cambridge Univ. Press, Cambridge, UK*, (1993).
- [12] I. Ciufolini, “Dragging of inertial frames”, *Nature*, **449**, 41 (2007) and references therein.
- [13] L. Iorio, “An Assessment of the Systematic Uncertainty in Present and Future Tests of the Lense-Thirring Effect with Satellite Laser Ranging”, *Space Sci. Rev.* **148**: 363381, (2009).
- [14] J. B. Hartle, *Gravity: An introduction to Einstein’s General relativity*, Pearson (2009).
- [15] H. Pfister, “On the history of the so-called Lense-Thirring effect”, *Gen. Rel. Grav.* **39**: 1735-1748 (2007).
- [16] D. Bini, A. Geralico, R. T. Jantzen, “Gyroscope precession along bound equatorial plane orbits around a Kerr black hole” *Phys. Rev. D* **94**, 064066 (2016).
- [17] C. Chakraborty & P. Majumdar, “ Strong gravity Lense-Thirring precession in Kerr and Kerr-Taub-NUT spacetimes” , *Class. Quantum Grav.*, **31** 075006 (2014).
- [18] C. Chakraborty & P. Pradhan, “Lense-Thirring precession in Plebański-Demiański Spacetimes”, *Eur. Phys. J. C* , **73** 2536 (2013).
- [19] C. Chakraborty & P. Pradhan, “ Behavior of a test gyroscope moving towards a rotating traversable wormhole ”, *JCAP* **003** , 035 (2017).
- [20] C. Chakraborty et al., “ Dragging of inertial frames inside the rotating neutron stars ”, *The Astrophysical J.*, **790**:2 (2014).
- [21] D. Chatterjee et al., “ Gravitomagnetic effect in magnetized neutron stars ”, *JCAP* **01**, 062 (2017).
- [22] S. M. Morsink & L. Stella, “ Relativistic precession around rotating neutron stars: Effects due to frame-dragging and stellar oblateness ”, *The Astrophysical J.*, **513** 827 (1999).
- [23] C. Chakraborty et al., “ Distinguishing Kerr naked singularities and black holes using the spin precession of a test gyro in strong gravitational fields”, *Phys. Rev. D* **95**, 084024 (2017).
- [24] C. Chakraborty et al., “Inertial Frame Dragging in an Acoustic Analogue Spacetime”, *Ann. Phys. (Berlin)*, 1700231, (2017).
- [25] J. W. Moffat, “Black Holes in Modified Gravity”, *Eur. Phys. J. C* **75** 175 (2015).
- [26] J. W. Moffat, “Scalar-Tensor-Vector Gravity Theory”, *JCAP* **0603**, 004 (2006).
- [27] J. W. Moffat, “Modified Gravity Black Holes and their Observable Shadows”, *Eur. Phys. J. C* **75** 130 (2015).
- [28] J. R. Mureika et al., “Black Hole Thermodynamics in Modified Gravity”, *Phys. Lett. B* **757**, 528 (2016).

- [29] M. F. Wondrak et al., “Superradiance in Modified Gravity (MOG)”, *JCAP* **021**, (2018).
- [30] J. W. Moffat & V. T. Toth, “The bending of light and lensing in modified gravity”, *MNRAS* **397**, 1885 (2009).
- [31] L. Manfredi et al., “Quasinormal modes of modified gravity (MOG) black holes”, *Phys. Lett. B* **779**, 492 (2018).
- [32] P. Pradhan, “Area (or Entropy) Products in Modified Gravity and Kerr-MOG/CFT Correspondence”, *The Euro. Phys. J. Plus*, **133**, 187 (2018).
- [33] S. W. Wei & Y. X. Liu, “Merger estimates for rotating Kerr black holes in modified gravity”, *Phys. Rev. D* **98**, 024042 (2018).
- [34] P. Sheoren et al., “Mass and spin of a Kerr black hole in modified gravity and a test of the Kerr black hole hypothesis ”, *Phys. Rev. D*, **97** 124049 (2018).
- [35] P. Pradhan, “Study of energy extraction and epicyclic frequencies in Kerr-MOG (Modified Gravity) black hole”, *Eur. Phys. J. C* , **79** 401 (2019).
- [36] C. Chakraborty et al., “Spin precession in a black hole and naked singularity spacetime”, *Phys. Rev. D* **95**, 044006 (2017).
- [37] D. Pugliese et al., “Equatorial circular orbits of neutral test particles in the Kerr-Newman spacetime”, *Phys. Rev. D* **88**, 024042 (2013).
- [38] F. de Felice, “Classical instability of a naked singularity”, *Nature* **273**, 8 (1978).
- [39] M. Calvini et al., “Are Naked Singularities Really Visible?”, *Lett. Nuovo Cimento*, **23** 15 (1978).
- [40] H. Zhang, “Naked Singularity, firewall, and Hawking radiation”, *Scientific Reports*, **7** 4000 (2017).
- [41] D. Pugliese, H. Quevedo, “Disclosing connections between black holes and naked singularities: horizon remnants, Killing throats and bottlenecks”, *Eur. Phys. J. C* , **79** 209 (2019).
- [42] D. Pugliese, H. Quevedo, “Kerr metric bundles. Killing horizons confinement, light-surfaces and horizons replicas”, arXiv: 2005.04130.
- [43] N. Straumann, *General Relativity with applications to Astrophysics*, Springer (2009).
- [44] A. Strominger and C. Vafa, “ Microscopic origin of the Bekenstein-Hawking entropy” *Phys. Lett. B.* **379** 99 (1996).
- [45] R. T. Jantzen, P. Carini & D. Bini, “The Many Faces of Gravitoelectromagnetism, *Annals Phys.* **215**, 1 (1992).
- [46] J. M. Bardeen, “A Variational Principle for Rotating Stars in General Relativity”, *Astrophys. J.* **162**, 71 (1970).
- [47] J. M. Bardeen, W. H. Press & S. A. Teukolsky, “Rotating Black Holes: Locally Non-rotating Frames, Energy Extraction, and Scalar Synchrotron Radiation”, *Astrophys. J.* **178**, 347 (1972).
- [48] A. Maselli et al., “Geodesic models of quasi-periodic-oscillations as probes of quadratic gravity”, *Astrophysical Journal*, **1**, 843 (2017).
- [49] L. Stella et al., “Correlations in the QPOs frequencies of low mass x-ray binaries and the relativistic precession model”, *Astrophysical Journal*, **L63-L66**, 524 (1999).
- [50] G. Török & Z. Stuchlik, “Radial and vertical epicyclic frequencies of Keplerian motion in the field of Kerr naked singularities”, *Astronomy and Astrophysics* **437**, 775 (2005).

- [51] K. Sakina & J. Chiba, “Parallel transport of a vector along a circular orbit in Schwarzschild space-time”, *Phys. Rev. D* **19**, 2280 (1979).
- [52] I. V. Tanatarov, O. B. Zaslavskii, “Collisional super-Penrose Process and Wald inequalities”, *Gen. Relat. Gravit.* **49**, 119 (2017).
- [53] C. W. Misner, K. S. Thorne & J. A. Wheeler, *Gravitation*, *W. H. Freeman & Company* (1973).
- [54] D. D. Doneva et al., “Orbital and epicyclic frequencies around rapidly rotating compact stars in scalar-tensor theories of gravity”, *Phys. Rev. D* **90**, 044004 (2014).
- [55] C. Chakraborty & P. Pradhan, “ Behavior of a test gyroscope moving towards a rotating traversable wormhole”, *JCAP* **03**, 035 (2017).